Contribution of expanded marine sulfur chemistry to the seasonal variability of DMS oxidation products and size-resolved sulfate aerosol

Linia Tashmim[1], William C. Porter[1], Qianjie Chen[2], Becky Alexander[3], Charles H. Fite[4], Christopher D. Holmes[4], Jeffrey R. Pierce[5], Betty Croft[6], and Sakiko Ishino[7]

[1]Department of Environmental Sciences, University of California, Riverside, CA, USA
[2]Department of Civil and Environmental Engineering, The Hong Kong Polytechnic University, Hong Kong, China
[3]Department of Atmospheric Sciences, University of Washington, Seattle, WA, USA
[4]Department of Earth, Ocean and Atmospheric Science, Florida State University, Tallahassee, FL, USA
[5]Department of Atmospheric Science, Colorado State University, Fort Collins, CO, USA
[6]Department of Physics and Atmospheric Science, Dalhousie University, Halifax, Nova Scotia, Canada
[7]Institute of Nature and Environmental Technology, Kanazawa University, Japan

Correspondence: Linia Tashmim (ltash001@ucr.edu) and William C. Porter (william.porter@ucr.edu)

Abstract. Marine emissions of dimethyl sulfide (DMS) and the subsequent formation of its oxidation products methane sulfonic acid (MSA) and sulfuric acid (H_2SO_4) are well-known natural precursors of atmospheric aerosols, contributing to particle mass and cloud formation over ocean and coastal regions. Despite a long-recognized and well-studied role in the marine troposphere, DMS oxidation chemistry remains a work in progress within many current air quality and climate models, with recent advances exploring heterogeneous chemistry and uncovering previously unknown intermediate species. With the identification of additional DMS oxidation pathways and intermediate species influencing its eventual fate, it is important to understand the impact of these pathways on the overall sulfate aerosol budget and aerosol size distribution. In this work, we update and evaluate the DMS oxidation mechanism of the chemical transport model GEOS-Chem by implementing expanded DMS oxidation pathways into the model. These updates include gas- and aqueous-phase reactions, the formation of the intermediates dimethyl sulfoxide (DMSO) and methane sulphinic acid (MSIA), as well as cloud loss and aerosol uptake of the recently quantified intermediate hydroperoxymethyl thioformate (HPMTF). We find that this updated mechanism collectively decreases the global mean surface-layer gas-phase sulfur dioxide (SO_2) mixing ratio by 35% and enhances sulfate aerosol (SO_4^{2-}) mixing ratio by 22%. We further perform sensitivity analyses exploring the contribution of cloud loss and aerosol uptake of HPMTF to the overall sulfur budget. Comparing modeled concentrations to available observations we find improved biases relative to previous studies. To quantify impacts of these chemistry updates on global particle size distributions and mass concentration we use the TOMAS aerosol microphysics module coupled to GEOS-Chem, finding changes in particle formation and growth affect the size distribution of aerosol. With this new DMS-oxidation scheme the global annual mean surface layer number concentration of particles with diameters smaller than 80 nm decreases by 12.8%, with cloud loss processes related to HPMTF mostly responsible for this reduction. However, global annual mean number of particles larger than 80 nm increases by 3.1%, suggesting that the new scheme promotes seasonal particle growth to these sizes capable of acting as cloud condensation nuclei (CCN).

1 Introduction

Dimethyl sulfide (DMS: CH_3SCH_3) is the most abundant biological source of sulfate aerosol and has a significant influence on Earth's radiation budget and climate due to its contribution to atmospheric marine particle (Charlson et al., 1987; Fung et al., 2022). In the atmosphere, DMS reacts with hydroxyl radical (OH), nitrate radical (NO_3), ozone (O_3) and various halogen species (e.g., chlorine (Cl) and bromine oxide (BrO)), primarily forming sulfur dioxide (SO_2) and methyl sulfonic acid (MSA; CH_3SO_3H) (Chen et al., 2018; Faloona, 2009; Hoffmann et al., 2016). These oxidation products are considered key influences on the formation and evolution of natural aerosols and clouds along with their associated climate impacts, especially in the marine boundary layer (MBL) (Carslaw et al., 2013; Sipilä et al., 2010; Schobesberger et al., 2013; Thomas et al., 2010; von Glasow and Crutzen, 2004). SO_2 and MSA formed by DMS oxidation can be deposited on Earth surface or further oxidize affecting the size distribution of aerosol and cloud microphysics (Leaitch et al., 2013; Wollesen de Jonge et al., 2021). SO_2 can either oxidize in the gas-phase by reaction with the OH radical forming H_2SO_4, which can participate in nucleation and early growth of particles in the atmosphere, or it can be taken up by cloud droplets and undergo aqueous phase oxidation by reaction with H_2O_2, O_3 and O_2 catalyzed by transition metals (Mn, Fe) forming SO_4^{2-} and generally only contributing to the growth of aerosol particles (Hoyle et al., 2016; Kulmala, 2003; Alexander et al., 2009). The hypohalous acids (HOBr, HOCl, HOI) also plays significant role in aqueous-phase sulfate production in the marine boundary layer (MBL) (Chen et al., 2016; Sherwen et al., 2016b). Recent studies have highlighted the importance of natural aerosols originating from DMS oxidation and their contribution to the uncertainty of aerosol radiative forcing in climate models (Carslaw et al., 2013; Fung et al., 2022; Rosati et al., 2022; Novak et al., 2021, 2022). Since DMS-derived aerosol is a major source of uncertainty in estimating the global natural aerosol burden and associated aerosol indirect radiative forcing, a more accurate representation of DMS oxidation and particle formation processes is an important step towards improved Earth system and climate modeling.

Although the chemistry of DMS oxidation has been previously studied in great detail, known uncertainties and omissions in the current mechanism remain in current air quality and chemical transport models (Barnes et al., 2006; Fung et al., 2022; Hoffmann et al., 2016, 2021). Furthermore, while increasingly complex and experimentally validated mechanisms are under ongoing development, DMS oxidation processes in many current chemical transport models continue to be represented through simplified gas-phase reactions with the tropospheric oxidants OH and NO_3, producing the two major oxidation products SO_2 and MSA at a fixed ratio as shown in R1-R3 in Table 1 (Chen et al., 2018; Chin et al., 1996; Veres et al., 2020). This type of simplified mechanism neglects the formation and loss of important intermediates such as dimethyl sulfoxide (DMSO: CH_3SOCH_3), methane sulphinic acid (MSIA: CH_3SO_2H) and the recently discovered oxidation product hydroperoxymethyl thioformate (HPMTF: $HOOCH_2SCHO$) (Berndt et al., 2019; Veres et al., 2020; Wu et al., 2015; Khan et al., 2021).

These omissions can have major consequences on product yields of DMS oxidation, thereby affecting the aerosol burdens. For example, the OH-addition pathway of DMS forms DMSO and MSIA as the intermediates, which has been identified as a dominant source of MSA via their aqueous-phase oxidation, and a fraction of that MSA subsequently undergoes aqueous-phase oxidation to form sulfate aerosol (Chen et al., 2018; Ishino et al., 2021; Zhu et al., 2006; von Glasow and Crutzen, 2004). Previous studies suggest that BrO contributes to 8 – 30% of total DMS loss, highlighting the importance of this pathway as well (Breider et al., 2010; Boucher et al., 2003; Chen et al., 2018; Khan et al., 2016). More recent experimental and laboratory studies have confirmed the formation of methylthiomethyl peroxy radicals (CH_3CH_2OO; abbreviated as MSP or MTMP) from the H-abstraction channel of OH oxidation, which can subsequently lead to a series of rapid intramolecular H-shift isomerization reactions, ultimately resulting in the formation of the stable intermediate HPMTF (Berndt et al., 2019; Veres et al., 2020; Vermeuel et al., 2020; Wu et al., 2015; Fung et al., 2022; Jernigan et al., 2022a). It has been reported that 30–46% of emitted DMS forms HPMTF according to different modeling studies and this falls within the observational range from NASA Atmospheric Tomography ATom-3 and ATom-4 flight campaigns where about 30–40% DMS was oxidized to HPMTF along their flight tracks (Fung et al., 2022; Veres et al., 2020; Novak et al., 2021). Subsequent investigation of the isomerization rate and heterogeneous loss of HPMTF in cloud droplets and aerosol shows a high production rate of marine carbonyl sulfide (OCS) from the chemical loss of HPMTF, a potential precursor of stratospheric sulfate aerosol and significant inhibitor of cloud condensation nuclei (CCN) formation due to the resulting reduction of surface SO_2 (Jernigan et al., 2022a). With the latest experimental findings on heterogeneous loss process of HPMTF and experimentally validated oxidation reactions for OCS formation directly from HPMTF it is necessary to include these reactions as part of the DMS oxidation mechanism as these will have impact on overall yield of SO_2, thus affecting the formation probability of CCN (Jernigan et al., 2022a, b).

Table 1. The three DMS oxidation reactions in the standard GEOS-Chem chemical mechanism

Reactions	**Rate (s^{-1})**	
DMS+ $OH_{(abstraction)} \rightarrow SO_2 + CH_3O_2 + CH_2O$	1.20e-11*exp(-280/T)	(R1)
DMS+ $OH_{(addition)} \rightarrow 0.75\ SO_2 + 0.25$ MSA + CH_3O_2	$8.2\times10^{-39}[O_2]e^{5376/T}/(1+1.05\times10^{-5}([O2]/[M])e^{3644/T})$ $cm^3 molecule^{-1}s^{-1}$	(R2)
DMS+ $NO_3 \rightarrow SO_2 + HNO_3 + CH_3O_2 + CH_2O$	1.90e-13*exp(530/T)	(R3)

Considering these and other consequences of complex DMS oxidation processes, a heavily simplified oxidation scheme will necessarily neglect potentially important reaction intermediates along with their production and loss pathways, with implications for the concentration and distribution of the oxidation products, including particulate sulfate. Differing intermediate lifetimes further influence sulfur removal and transport depending on the relative dominance of pathways. Thus, the exclusion of key pathways and intermediate species can lead to errors in the representation of the spatial distribution of both gas- and particle-phase sulfur species, as well as global sulfur burden.

The DMS oxidation products sulfate and MSA play an important role in Earth's radiative budget through cloud droplet formation, and the extent of this role depends on how efficiently they can produce and grow new particles in the marine atmosphere (Thomas et al., 2010). SO_2 can oxidize in the gas-phase the forming H_2SO_4, which acts as a key product contributing to nucleation and condensational growth as shown in Figure 1. SO_2 oxidizing through aqueous chemistry in cloud droplets does contribute to particle growth rates by providing larger aerosol during cloud evaporation that acts as more efficient CCN (Kaufman and Tanré, 1994). On the other hand, MSA might participates in nucleation along with sulfuric acid in presence of amines or ammonia (Johnson and Jen, 2023). Recent studies have highlighted the importance of aqueous-phase chemistry in the formation and loss of MSA (Boniface et al., 2000; Chen et al., 2015; Kaufman and Tanré, 1994; Kulmala et al., 2000).

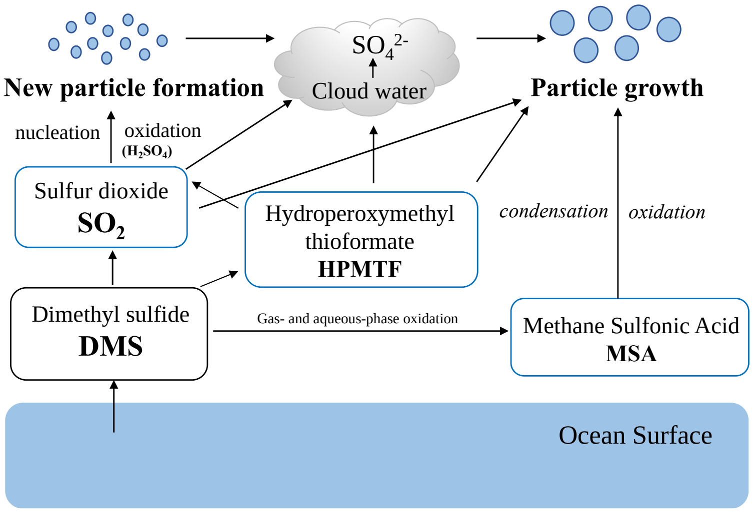

Figure 1 Modified DMS oxidation mechanism used in this work (simulation MOD) showing the formation of major stable oxidation products (blue-outline boxes) including newly identified intermediate HPMTF, and their contribution to new particle formation or growth of existing particles. Note that we include gas-phase and aqueous-phase chemistry of DMSO, MSIA and OCS in the mechanism, which counts towards their contribution to the formation of major oxidation products of DMS, but that these pathways are not explicitly shown here to maintain visual clarity.

Additionally, the recently identified intermediate HPMTF also has the potential for further gas-phase oxidation. Under cloud-free conditions, HPMTF can undergo gas-phase oxidation by OH, producing SO_2 and eventually leading to the formation of non-sea-salt-SO_4^{2-}. This sulfate can contribute to aerosol formation and growth processes, with climate implications (Galí et al., 2019). Other work has used direct airborne eddy covariance flux measurements to explain the chemical fate of HPMTF in the MBL, finding that in cloudy conditions chemical loss due to aqueous phase reactions in clouds is the major HPMTF removal process (Novak et al., 2021). In the same study, global model simulations showed a 35% reduction in global annual average SO_2 production from DMS and a 24% reduction in the near-surface (0 to 3 km) global annual average SO_2 concentrations over the ocean as a result of this process (Novak et al., 2021). Thus, a complete representation of cloud loss and aerosol uptake is needed to effectively evaluate the atmospheric impacts of marine DMS and their connections to cloud formation (Novak et al., 2021; Holmes et al., 2019).

To better understand the marine sulfur budget, as well as the eventual formation, size distribution, and seasonality of sulfate aerosol, we use the global chemical transport model GEOS-Chem, integrating previously developed mechanisms along with newly proposed pathways involving the formation and loss of the intermediates DMSO, MSIA, and HPMTF. As part of this work, we further quantify the atmospheric impacts of individual reactions and mechanisms, evaluate uncertainties in the chemical mechanism, and identify improvements necessary to better represent the impacts of DMS more accurately on atmospheric chemistry and climate. The resulting integrated scheme provides a more complete representation of marine sulfur and sulfate aerosol species in marine tropospheric environments compared to the simplified base GEOS-Chem mechanism, with improved comparisons to aircraft and surface observations. Since aerosols are a major contributor to uncertainty in climate forcing, improving oxidation and aerosol formation mechanisms by adding and optimizing neglected reactions in models is a crucial step towards a more mechanistically robust representation of particle yields and sensitivities. We further perform multiple sensitivity tests to investigate how the uncertainty in heterogeneous uptake of the newly identified HPMTF could influence DMS chemistry and tropospheric aerosol formation (Holmes et al., 2019; Novak et al., 2021). In a broader sense our work provides a more detailed story on the heterogeneous loss, fate, and ultimate impacts of DMS and its oxidation products, improving our understanding of a key ocean-atmosphere interaction in the context of global change.

2 Methodology

To simulate DMS chemistry and its oxidation products GEOS-Chem global chemical transport model v12.9.3 is used. Impacts on simulated aerosol size, number and mass concentration are considered by coupling the TwO-Moment Aerosol Sectional (TOMAS) aerosol microphysics module with GEOS-Chem v12.9.3 (GC-TOMAS) (https://github.com/geoschem/geos-chem/tree/12.9.3) (Adams and Seinfeld, 2002; Kodros and Pierce, 2017). The default GEOS-Chem chemical mechanism contains detailed HO_x–NO_x–VOC–O_3–halogen tropospheric chemistry along with recently updated halogen chemistry and in-cloud processing (Bey et al., 2001; Holmes et al., 2019; Chen et al., 2017; Parrella et al., 2012; Schmidt et al., 2016; Wang et al., 2019). The DMS emission flux from ocean are controlled by a gas transfer velocity which is dependent on sea surface temperature and wind speed (Johnson, 2010) and a climatology of concentrations in seawater (Lana et al., 2011; Nightingale et al., 2000). The aqueous-phase concentration of O_3 in aerosols or cloud droplets is calculated assuming gas-liquid equilibrium and aqueous-phase concentration of OH is calculated following $[OH_{(aq)}] = \delta[OH_{(g)}]$ where, $\delta = 1 \times 10^{-19}$ M cm^3 $molecule^{-1}$ (Jacob et al., 2005; Chen et al., 2018).

In this study, TOMAS tracks aerosol number and the mass of each aerosol species in 15 logarithmically sized bins, with sizes in this analysis ranging from 3 nm to 10 µm (Lee and Adams, 2012; Lee et al., 2013). All binned aerosol species undergo interactive microphysics, allowing the calculation of aerosol number budgets (Westervelt et al., 2013). The version of GC-TOMAS used here includes 47 vertical levels, a horizontal resolution of 4° × 5°, and the GEOS-FP data product for meteorological inputs. Simulations are performed for 2018, with 11 months of discarded model spin up. Nucleation is simulated via a ternary nucleation scheme involving water, sulfuric acid, and ammonia with nucleation rates scaled by 10^{-5} (Napari et al., 2002; Westervelt et al., 2013). In low-ammonia regions (less than 1 pptv), a binary nucleation scheme involving water and sulfuric acid is instead used (Vehkamäki et al., 2002). Previously GC-TOMAS has been used for aerosol simulations to investigate topics such as the aerosol cloud-albedo effect and cloud condensation nuclei formation (Kodros et al., 2016; Kodros and Pierce, 2017; Pierce and Adams, 2006; Westervelt et al., 2013). Aerosol species available for GC-TOMAS simulations are sulfate, aerosol water, black carbon, organic carbon, mineral dust, and sea salt (Alexander et al., 2005; Bey et al., 2001; Duncan Fairlie et al., 2007; Pye et al., 2009). The wet and dry deposition scheme for aerosols and gas species are based on previous studies (Amos et al., 2012; Emerson et al., 2020; Liu et al., 2001; Wesely, 1989; Wang et al., 1998).

We refer to simulations performed using only these three DMS oxidation reactions (Table 1) as the “BASE”, involving only the direct formation of SO_2 and MSA in gas-phase (Chin et al., 1996). We further implement and evaluate a custom chemical mechanism for DMS oxidation, referred to as “MOD” (Table 2-4), representing an integration of three individual DMS oxidation mechanism updates explored previously using GEOS-Chem and CAM6-Chem, along with HPMTF loss via heterogenous chemistry in clouds and aerosols and dry and wet deposition of HPMTF (Chen et al., 2018; Fung et al., 2022; Veres et al., 2020; Novak et al., 2021). Loss of HPMTF in clouds follow entrainment-limited uptake which used a chemical rate expression to control rate of mixing between cloudy and clear air (Holmes et al., 2019). In GC-TOMAS we use specific subroutine that take amount of sulfate produced via in-cloud oxidation and condense it into an existing aerosol size distribution. So, mass of sulfate produced by oxidation is portioned to the various size bins according to the number of particles in that size bin. TOMAS microphysics accounts for H_2SO_4

formation based on gas-phase oxidation of SO_2 included in the kinetic preprocessor (KPP) equation list valid for the simulation BASE. Since there are additional sources of sulfate in the integrated DMS oxidation mechanism both in gas and aqueous phase, we made necessary changes in the KPP code to explicitly track H_2SO_4 formation by gas phase oxidation of SO_2. On the other hand, code changes for sulfate formed by heterogeneous oxidation of MSA and HPMTF (in clouds and aerosols) were added in the GEOS-Chem microphysics module that also handles in-cloud oxidation of SO_2 in GC version 12.9.3 (Park et al., 2004; Trivitayanurak et al., 2008).

Table 2. Overview of the DMS oxidation mechanism via OH-addition pathway.

Gas-phase reactions	**Rate (s^{-1})**	**References**
DMS + OH → $0.60SO_2$ + 0.4DMSO + CH_3O_2	$8.2\times10^{-39}[O_2]e^{5376/T}/(1+1.05\times10^{-5}([O2]/[M])e^{3644/T})$ $cm^3 molecule^{-1} s^{-1}$	(Burkholder et al., 2015; Pham et al., 1995; Spracklen et al., 2005)
DMS + BrO → DMSO + Br	1.50e-14*exp(1000/T)	(Bräuer et al., 2013; Hoffmann et al., 2016)
DMS + O_3 → SO_2	1.50e-19	(Burkholder et al., 2015; Du et al., 2007)
DMSO + OH → 0.95MSIA + $0.05SO_2$	6.10e-12*exp(800/T)	(Burkholder et al., 2015; von Glasow and Crutzen, 2004)
MSIA + OH → $0.9SO_2$ + 0.1MSA	9.00e-11	(Burkholder et al., 2015)
MSIA + O_3 → MSA	2.00e-18	(von Glasow and Crutzen, 2004; Lucas and Prinn, 2002)

Aqueous-phase reactions	**k_{298} [$M^{-1}s^{-1}$]**	**References**
DMS (aq) + O_3 (aq) → DMSO (aq) + O_2 (aq)	8.61×10^{8}	(Gershenzon et al., 2001; Hoffmann et al., 2016)
DMSO (aq) + OH (aq) → MSIA (aq)	6.65×10^{9}	(Zhu et al., 2003; Hoffmann et al., 2016)
MSIA (aq) + OH (aq) → MSA (aq)	6.00×10^{9}	(Sehested and Holcman, 1996; Hoffmann et al., 2016)
MSI^- (aq) + OH (aq) → MSA (aq)	1.20×10^{10}	(Bardouki et al., 2002; Hoffmann et al., 2016)
MSIA (aq) + O_3 (aq) → MSA (aq)	3.50×10^{7}	(Hoffmann et al., 2016)
MSI^- (aq) + O_3 (aq) → MSA (aq)	2.00×10^{6}	(Flyunt et al., 2001; Hoffmann et al., 2016)
MSA (aq) + OH (aq) → SO_4^{2-}	1.50×10^{7}	(Hoffmann et al., 2016)
MS^- (aq) + OH (aq) → SO_4^{2-} (aq)	1.29×10^{7}	(Zhu et al., 2003; Hoffmann et al., 2016)

Table 3. Overview of the DMS oxidation mechanism involving HPMTF formation.

Gas-phase reactions	**Rate (s^{-1})**	**References**
MSP (CH_3SCH_2OO) → $OOCH_2SCH_2OOH$	2.2433e11*exp(-9.8016e3/T)*(1.0348e8/T^3)	(Berndt et al., 2019; Veres et al., 2020; Wollesen de Jonge et al., 2021)
$OOCH_2SCH_2OOH$ → HPMTF ($HOOCH_2SCHO$) + OH	6.0970e11*exp(-9.489e3/T)*(1.1028e8/T^3)	(Berndt et al., 2019; Veres et al., 2020; Wollesen de Jonge et al., 2021)
$OOCH_2SCH_2OOH$ + NO → $HOOCH_2S$ + NO_2 + HCHO	4.9e-12*exp(260/T)	(Saunders et al., 2003)
MSP + HO_2 → CH_3SCH_2OOH + O_2	1.13e-13*exp(1300/T)	MCMv3.3.1, (Wollesen de Jonge et al., 2021)
CH_3SCH_2OOH + hv → CH_3SCH_2O +OH	J(41)	MCMv3.3.1, (Wollesen de Jonge et al., 2021)
HPMTF + OH→ $HOOCH_2SCO$ + H_2O	4.00e-12	(Jernigan et al., 2022a)

HPMTF + OH$\rightarrow$ 0.13OCS + 0.87SO_2 + CO	1.40e-11	(Jernigan et al., 2022a)
OCS + OH $\rightarrow$ SO_2	1.13e-13*exp(1200/T)	(Jernigan et al., 2022a)
$HOOCH_2SCO \rightarrow HOOCH_2S$ + CO	9.2e9*exp(-505.4/T)	(Wu et al., 2015)
$HOOCH_2SCO \rightarrow OH + CH_2O$ + OCS	1.6e7*exp(-1468.6/T)	(Wu et al., 2015)
$HOOCH_2S + O_3 \rightarrow HOOCH_2SO + O_2$	1.15e-12*exp(430/T)	(Saunders et al., 2003)
$HOOCH_2S + NO_2 \rightarrow HOOCH_2SO$ + NO	6.0e-11*exp(240/T)	(Saunders et al., 2003)
$HOOCH_2SO + O_3 \rightarrow SO_2 + CH_2O + OH + O_2$	4.0e-13	(Saunders et al., 2003)
$HOOCH_2SO + NO_2 \rightarrow SO_2 + CH_2O$ + OH + NO	1.2e-11	(Saunders et al., 2003)

Table 4. Overview of the MSA-producing branch of the H-abstraction pathway of DMS oxidation.

Gas-phase reactions	**Rate (s^{-1})**	**Original References**
DMS + OH $\rightarrow$ MSP (CH_3SCH_2OO) + H_2O	1.12e-11*exp(-250/T)	(Saunders et al., 2003)
DMS + Cl $\rightarrow$ 0.45MSP + 0.55C_2H_6SCl + 0.45HCl	3.60e-10	(Fung et al., 2022; Enami et al., 2004)
$C_2H_6SCl \rightarrow$ DMSO + ClO	4.00e-18	(Hoffmann et al., 2016)
DMS + $NO_3 \rightarrow$ MSP + HNO_3	1.9e-13*exp(520/T)	(Novak et al., 2021; Wollesen de Jonge et al., 2021)
MSP + NO $\rightarrow CH_3SCH_2(O) + NO_2$	4.9e-12*exp(260/T)	(Saunders et al., 2003)
MSP + $CH_3O_2 \rightarrow CH_3SCH_2(O) + O_2$	3.74e-12	(Saunders et al., 2003)
$CH_3SCH_2(O) \rightarrow CH_3S + CH_2O$	1.0e6	(Saunders et al., 2003)
$CH_3S + O_3 \rightarrow CH_3S(O) + O_2$	1.15e-12*exp(430/T)	(Saunders et al., 2003)
$CH_3S + O_2 \rightarrow CH_3S(OO)$	1.20e-16*exp(1580/T)	(Saunders et al., 2003)
$CH_3S(O) + O_3 \rightarrow CH_3(O_2) + SO_2$	4.00e-13	(Saunders et al., 2003)
$CH_3S(OO) \rightarrow CH_3(O_2) + SO_2$	5.60e16*exp(-10870/T)	(Saunders et al., 2003)
$CH_3S(OO) \rightarrow CH_3SO_2$	1.00	(Saunders et al., 2003)
$CH_3SO_2 + O_3 \rightarrow CH_3SO_3 + O_2$	3.00e-13	(Saunders et al., 2003)
$CH_3SO_2 \rightarrow CH_3(O_2) + SO_2$	5.00e13*exp(-9673/T)	(Saunders et al., 2003)
$CH_3SO_3 + HO_2 \rightarrow$ MSA + O_2	5.00e-11	(Saunders et al., 2003)
$CH_3SO_3 \rightarrow CH_3(O_2) + H_2SO_4$	5.00e13*exp(-9946/T)	(Saunders et al., 2003)

To examine the sensitivities of size-resolved aerosol formation and growth to DMS chemistry modifications, model simulations are conducted as summarized in Table 5. Output from simulations MOD and MOD_noHetLossHPMTF was then compared against simulation BASE to understand the contribution of these additional chemical reactions on spatial pattern of the surface concentration of major oxidation products of DMS.

Table 5. List of mechanisms used in GEOS-Chem-TOMAS simulations.

Model Runs	**Mechanism**	**HPMTF Cloud Loss**[*]	**HPMTF Aerosol Loss**[*]
BASE	All reactions from Table 1	-	-
MOD_noHetLossHPMTF	All reactions from Table 2-4	Off	Off
MOD	All reactions from Table 2-4	On	On

[*] Instantaneous formation of sulfate via HPMTF cloud and aerosol loss uses a reactive uptake co-efficient (γ) of 0.0016.

As shown in Table 2, the modified DMS chemistry simulations examined here include gas- and aqueous-phase oxidation of DMS and its intermediate oxidation products by OH, NO_3, O_3, and halogenated species as previously explored in an older version of GEOS-Chem (Chen et al., 2018). The aqueous-phase reactions in cloud droplets and aerosols were parameterized assuming a first-order loss of the gas-phase sulfur species (Chen et al., 2018). Further building upon this previous mechanism, the scheme used here also includes the formation and loss of HPMTF as previously tested in the global climate model CAM6-Chem as shown in Table 3 (Veres et al., 2020). Table 4 presents the third piece of the mechanism: a gas-phase MSA-producing branch of the H-abstraction pathway in the DMS chemistry bridging the other two sets of the reactions (Fung et al., 2022). A similarly integrated mechanism (Table 2-4) has been previously explored using the CAM6-Chem model with a focus on radiation budget impacts, with the exception of the DMS + NO_3 = MSP + HNO_3 reaction (included in Table 4) considered in this work (Fung et al., 2022; Novak et al., 2021; Wollesen de Jonge et al., 2021). We use a rate constant of 1.40×10^{-11} cm^3 $molecules^{-1}s^{-1}$ for HPMTF + OH, which was previously determined based concentrations of other known sulfur species (DMS, DMSO, SO_2 and methyl thioformate; MTF; CH_3SCHO; a structurally similar proxy to HPMTF) and evaluated by box model (Jernigan et al., 2022a). An exploration of reaction rate uncertainty for the HPMTF+OH reaction (Table 3), including both high and low end limits of 5.5×10^{-11} cm^3 $molecules^{-1}s^{-1}$ and 1.4×10^{-12} cm^3 $molecules^{-1}s^{-1}$ resulted in only minor impacts on the fate of HPMTF and ultimate sulfate formation in our simulations (Novak et al., 2021; Wu et al., 2015).

Model sensitivity simulations were also performed with (case "MOD") and without HPMTF heterogeneous uptake to clouds and aerosols (case "MOD_noHetLossHPMTF") to account for how much of the DMS-derived HPMTF eventually forms SO_2 in the presence of these additional loss processes (Table 5). Previous work shows that aerosol surface chemistry causes additional decreases in HPMTF mixing ratios, primarily over land, and that the loss of HPMTF in clouds is larger (36%) than losses from aerosols (15%) when using an uptake coefficient of $\gamma = 0.01$ for both processes (Novak et al., 2021). In this work, based on recent laboratory measurements, we use a smaller uptake coefficient ($\gamma = 0.0016$) for HPMTF loss to aerosols and clouds (Table 5) (Jernigan et al., 2022b). We assume HPMTF directly produces sulfate in cloud and aerosol followed but previous work even though there is uncertainty in the fate of HPMTF heterogeneous loss (Zhang and Millero, 1993; Novak et al., 2021; Jernigan et al., 2022a). For the aqueous-phase reactions listed in Table 2, including the oxidation of intermediates DMSO and MSIA in cloud droplets and aerosols, a first-order loss of the gas-phase sulfur species was assumed following previously used parameterizations and physical parameter values (Chen et al., 2018). Alongside the gas-phase and aqueous-phase reactions relevant to the added DMS oxidation mechanism contributing to the formation of SO_2 and sulfate, the default version of GC-TOMAS used here also includes in-cloud oxidation of SO_2 by H_2O_2, O_3, and O_2 catalyzed by transition metals (Mn, Fe), as well as the loss of dissolved SO_2 by HOBr and HOCl, all of which are passed to TOMAS to account for sulfate production (Chen et al., 2017; Wang et al., 2021).

All simulations are conducted for the year 2018, which was chosen to match the model simulation with the dates of the NASA Atmospheric Tomography flight campaign (ATom-4) offering observational data for HPMTF, DMS and SO_2. Rate coefficients for all gas-phase sulfur reactions are obtained from the most recent JPL report and other references while sulfur product yields for gas-phase reactions are obtained from various laboratory and modeling studies (Burkholder et al., 2020; Lucas and Prinn, 2002; Hoffmann et al., 2016; Gershenzon et al., 2001; Kowalczuk et al., 2003; Zhou et al., 2019; Jernigan et al., 2022a). The simulations included sea salt debromination except for some sensitivity tests described below (Zhu et al., 2019; Schmidt et al., 2016). In all our simulations including MOD, DMS is advected and undergoes chemical loss and transport but does not undergo dry or wet deposition. However, dry and wet deposition of oxidation products such as DMSO, MSIA, MSA and HPMTF are included.

We note that previous work has explored the impact of MSA on aerosol growth, including modifications within TOMAS to represent this process (Hodshire et al., 2019). We do not include this process here. Future work is recommended to examine its importance in the context of the chemistry updates presented here.

3 Result and discussion

3.1 Model-Observations Comparison

3.1.1 Surface DMS mixing ratio

We compared the modeled DMS mixing ratio averaged for each month with the observational data collected at Crete Island (35° N, 26° E) and Amsterdam Island (37° S, 77° E) (Kouvarakis and Mihalopoulos, 2002; Chen et al., 2018; Castebrunet et al., 2009). Comparing simulations BASE and MOD, we find a closer match with DMS observations for simulations using modified DMS chemistry for both observation data shown in Figure 2. Modeled DMS mixing ratios calculated using base chemistry show strong positive bias during the months of May and June for Crete Island. By comparison, during the same period the modeled DMS mixing ratios calculated with modified chemistry reduces the bias from 102% to 44%. Similarly, for Amsterdam Island major overpredictions are apparent for the BASE simulation compared to MOD for the months of May-August. One reaction that may play a role in this shift is DMS + BrO, which as indicated earlier is responsible for a faster overall chemical loss of DMS, in particular over the southern hemisphere high latitudes. Beside DMS chemistry, sea surface DMS concentration is also proven to affect the modeled DMS mixing ratio (Chen et al., 2018). But the aim of this study is to investigate the chemistry aspect of DMS oxidation, so we did not explored how change in DMS seawater climatology and thus their emission influence the surface DMS mixing ratio.

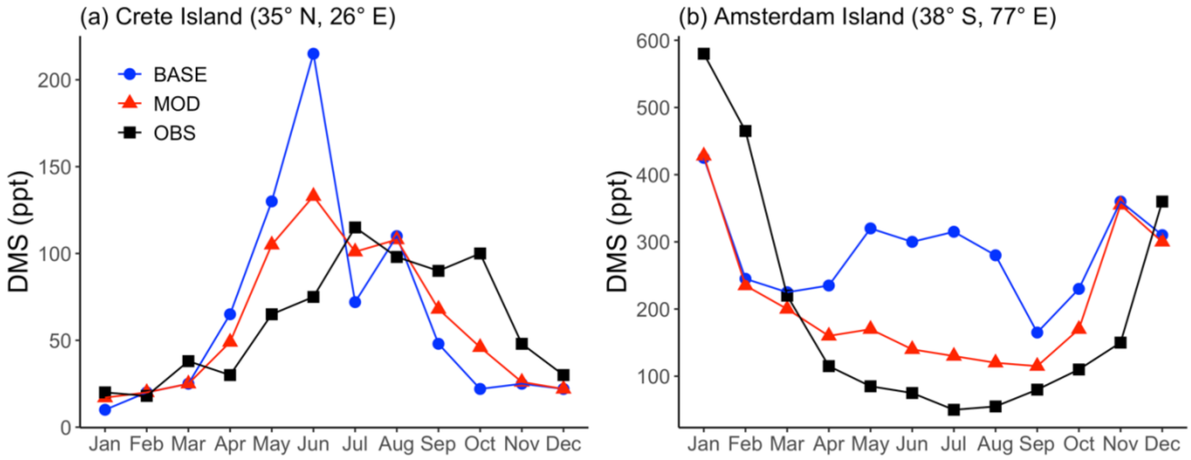

Figure 2 Observed (OBS) monthly mean surface DMS mixing ratios at (a) Crete Island and (b) Amsterdam Island compared with simulations BASE and MOD. Simulations are described in Table 5.

3.1.2 Comparison with aircraft observations

We further evaluate model output through a comparison with ATom-4 aircraft observations for specific days of measurement for DMS, HPMTF and SO_2 as shown in Figure 5. For this comparison, the model is sampled at the time and location of aircraft measurements by ATom-4 using the planeflight diagnostic of GEOS-Chem.

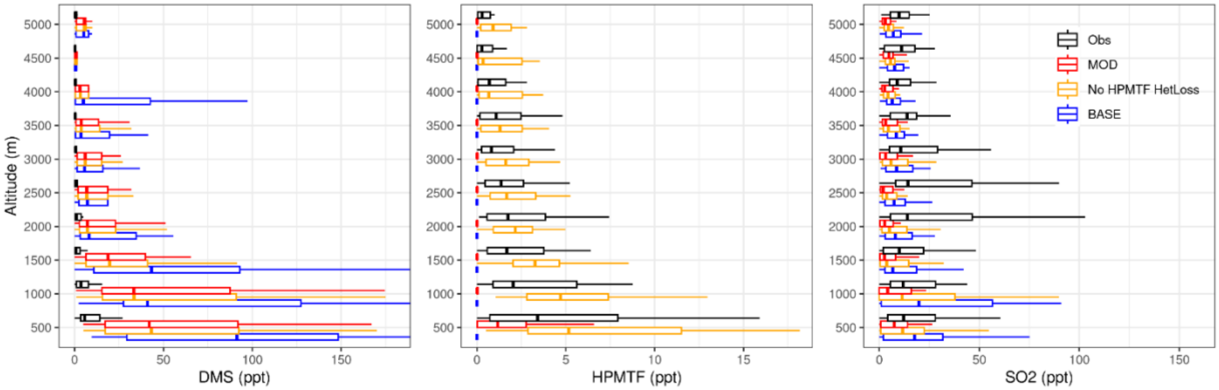

Figure 3 Vertical profiles of (a) DMS, (b) HPMTF and (c) SO_2 mixing ratios from ATom-4 observations (black) and model with simulation MOD sampled along the ATom-4 flight tracks (red) binned every 500 m of flight altitude. Also shown are modeled results without HPMTF heterogeneous loss with simulation MOD_noHetLossHPMTF (yellow), and for BASE GEOS-Chem chemistry (blue). Box plot whiskers show full range of distribution at each altitude bin. DMS observations are from Whole Air Samples (WAS) while HPMTF DC-8 observations are from iodide ion chemical ionization time-of-flight mass spectrometer (CIMS). SO_2 observations from ATom-4 campaign were measured by Laser Induced Fluorescence (LIF).

DMS concentrations measured during ATom-4 by whole air sampler (WAS) and modified chemistry simulation values for nearest neighbor grid cells are shown in Figure 3a across different altitude. In general, the modeled DMS concentrations are significantly higher than those observed during ATom-4 missions especially close to the surface. However, model DMS concentrations decrease more rapidly than the measurement with altitudes indicating vertical mixing could be one of the underlying reasons for this trend. Even with this near surface bias, simulation MOD relative to BASE has greater DMS losses and a shorter DMS lifetime (from 1.5 d to 1.0 d) reducing the gap between modeled and observed concentration compared to simulation BASE. The reduction in modeled DMS is largest over the Southern Ocean (shown later in Fig. 5b) where oxidation by BrO and O_3 in the aqueous phase plays the major role in reducing DMS concentration, thereby reducing the model-observation bias (Fig. 3b). Remaining model biases could be at least partially attributed to model uncertainty in oxidant concentrations and cloud cover. The heterogeneous loss of HPMTF has minimal impact on DMS concentration and its vertical profile.

For HPMTF, Figure 3b shows that the observed and modeled HPMTF concentrations remain largely below 15 ppt. Agreement between observations and modeled HPMTF mixing ratios in the vertical profile (Fig. 3b) is poor for simulation MOD even close to the surface. Removing all heterogeneous loss of HPMTF improves model comparisons aloft, though surface concentrations become overestimated (yellow line of Fig. 3b), showing a high sensitivity to cloud and aerosol loss processes. We also find that the modeled HPMTF:DMS ratios range from 0.15:1 to 0.5:1 on a daily basis in most cases for when there is no heterogeneous loss of HPMTF, compared to 0.5:1 observed during ATom-4 using the calibration maintained during measurement, implying reasonably good agreement for this value over daily time scales (Veres et al., 2020). The SARP flight campaign data has reported much lower HPMTF:DMS ratios (< 0.2) on cloudy days which is relatable to modeled HPMTF with simulation MOD (Novak et al., 2021). For simulation MOD, the modeled HPMTF:DMS ratio is 0.03:1 for until 0.5 km and then approaches zero with increasing altitude, indicating the need for additional work to better constrain production and loss processes of this intermediate. Our simulations indicate that cloud loss is the dominant modeled removal process of HPMTF, consistent with previous findings, while gas-phase OH oxidation plays a minor role (Novak et al., 2021). Thus, the addition of cloud uptake dramatically decreases HPMTF concentrations throughout the troposphere. Overall, this allows only 7% of HPMTF produced to end up as SO_2 with about 92% lost to clouds and aerosol and thus removed from the system, resulting net reduction in mean global SO_2 by about 35%. Previous work focusing entirely on gas-phase and heterogeneous loss of HPMTF shows a much higher bias for both DMS and HPMTF during cloudy and clear sky conditions using the same model and a condensed DMS oxidation mechanism, indicating that the addition of gas-phase and heterogeneous oxidation of DMS including additional intermediates such as DMSO and MSIA further reduce model biases for HPMTF with remaining overestimation of the multiphase loss for HPMTF (Novak et al., 2021).

We also compared the SO_2 concentrations measured during ATom-4 by Laser Induced Fluorescence (LIF) and simulation MOD values for nearest neighbor grid cells are shown in Figure 3c across different altitude. Modeled surface SO_2 concentrations are lower than those observed during ATom-4 missions across the vertical scale shown here for simulation MOD. The greater SO_2 losses results in a shorter SO_2 lifetime (from 1.4 d to 1.3 d) for simulation MOD relative to simulation BASE. The reduction in modeled SO_2 is largest over the Southern Ocean (shown later in Fig. 7a) where heterogeneous oxidation of HPMTF is most efficient and irreversible. Removing the heterogeneous loss of HPMTF increases the modeled SO_2 compared to simulation MOD with underprediction remaining for altitudes > 1km. Remaining model biases could be at least partially attributed to uncertainty in DMS oxidation processes along with other non-DMS sources contributing high concentration of SO_2. Aside from uncertainty in DMS emissions and oxidation, recent understanding of marine sulfur chemistry such as methanethiol (CH_3SH) oxidation has been reported as an significant source of SO_2 in the marine atmosphere and could help reduce the bias, a possibility deserving further investigation (Berndt et al., 2023; Novak et al., 2022). Overall the DMS oxidation chemistry implemented in this work reduces the model observation bias close to the surface (up to 1km) compared to BASE GEOS-Chem chemistry.

Besides the vertical profile shown in Figure 3b, the global mean surface mixing ratio of HPMTF with simulation MOD_noHetLossHPMTF for May 2018 is plotted in Figure 4 and compared with the observational measurement of HPMTF made during the ATom-4 mission during the NASA DC-8 flight campaign, which sampled the daytime remote marine atmosphere over the Pacific and Atlantic Oceans. The ATom-4 measurements were carried out during daytime hours between April 24 and May 21, 2018 for 21 non-continuous days.

For this campaign, flight patterns covered vertical profiles from 0.2 to 14 km above the ocean surface. The flight leg duration was 5 minutes and boundary layer altitude of 150 to 200 m above the ocean surface. Since most of these measurement days are within the month of May 2018, here we compare observations with modeled output of mean surface concentration of HPMTF for this month. With the rate of isomerization reaction used in previous work, we find spatial patterns of monthly mean surface concentrations are generally well captured (Jernigan et al., 2022a). Overall, we find that the simulation MOD_noHetLossHPMTF results in better agreement with existing overprediction for the vertical profile (Fig. 3b) and global surface layer HPMTF levels (Fig. 4) compared to previous modeled approaches using the CAM-chem model (Veres et al., 2020).

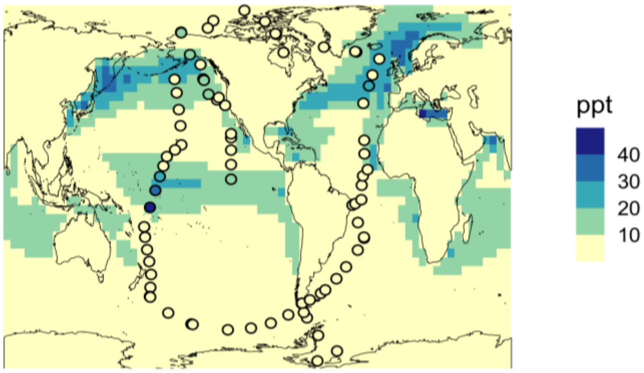

Figure 4 Geographic distribution of May 2018 monthly mean surface-layer mixing ratio of HPMTF for simulation MOD_noHetLossHPMTF mechanism represented for May 2018. The circles represent measurements of HPMTF during the ATom-4 mission by NASA DC-8 flight tracks with a limit of detection <1 ppt.

3.2 DMS burden and oxidation pathways

We find that the global burden of DMS in the MOD simulation is 67 Gg S (Table B1), 38% lower than what we find with the simulation BASE (108 Gg S). Even with this 38% reduction, global burdens are still well within the range of 9.6–150 Gg S suggested in other studies (Faloona, 2009; Kloster et al., 2006). Figure 5a shows that surface DMS mixing ratios are highest in the North Pacific and North Atlantic oceans for June-July-August (JJA) and in the Southern Ocean during the months of December-January-February (DJF), revealing the underlying seasonality of DMS emissions. According to previous studies, the highest DMS concentrations usually occur in summer months due to higher rates of primary production in the presence of adequate solar irradiation and high temperatures for both hemisphere (Galí et al., 2018; Lana et al., 2011; Wang et al., 2020). In simulation MOD, the global mean surface-layer DMS burden was higher in SH for DJF and lower in NH for JJA which is due to larger ocean area in the SH than NH. We also find that the reactions of this expanded DMS oxidation mechanism collectively contribute to reductions in mean surface-layer DMS concentration of 60% and 23% compared to BASE for JJA and DJF respectively (Fig. 5b). These reductions are due primarily to the addition of multiple new chemical loss pathways compared to BASE, which are especially impactful during JJA months due to due to elevated BrO in the SH winter and also higher O_3 and OH concentration in the NH summer compared to the SH summer (Zhang et al., 2018; Pound et al., 2020).

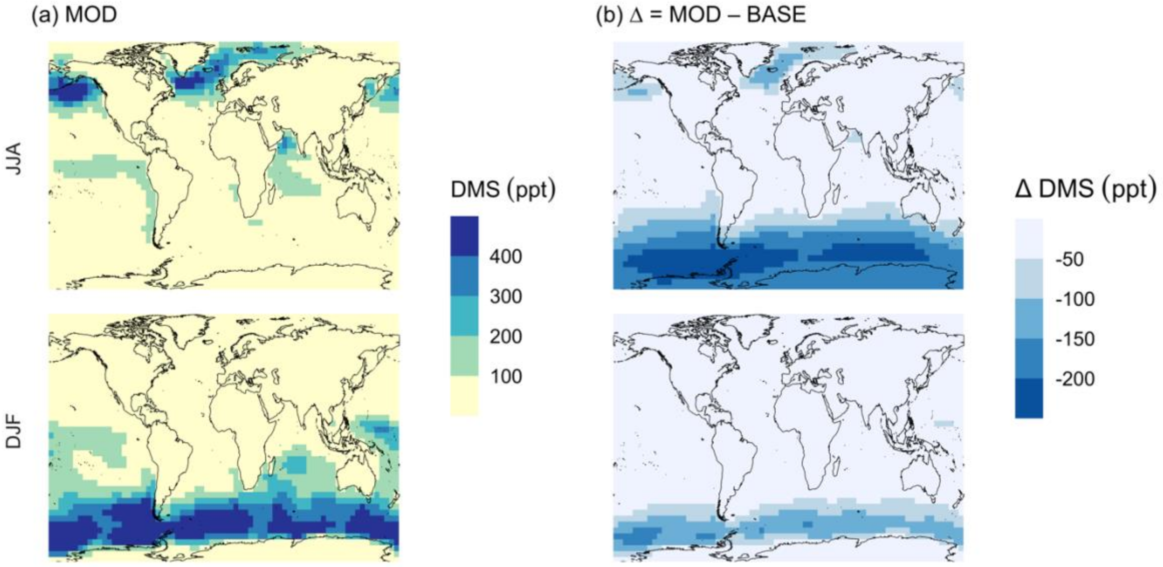

Figure 5 Geographic distribution of mean surface DMS mixing ratio (ppt) for simulation (a) MOD and (b) difference between simulations from its baseline, Δ = MOD – BASE from GEOS-Chem simulations. Here, JJA and DJF represent June-July-August and December-January-February respectively. Simulations are described in Table 5.

As shown in Fig. 5b, this DJF DMS reduction is seen mainly over the Southern Ocean and is largely attributable to faster chemical losses through the added reactions of DMS + BrO and $DMS_{(aq)}$ + $O_{3(aq)}$, which in earlier work was hypothesized as a possible reason for high model biases in the absence of detailed halogen chemistry (Chen et al., 2016). The global lifetime of DMS decreases from 1.5 days in the BASE simulation to 1.0 day in the MOD simulation.

These values are comparable to the range of 0.8–2.1 d reported by previous studies (Chen et al., 2018; Fung et al., 2022). The global DMS emission flux (F_{DMS}) from ocean to the atmosphere is 22 Tg S yr^{-1} and is within the range of 11– 28 Tg S yr^{-1} simulated by GEOS-Chem and other models in previous studies (Lennartz et al., 2015; Fung et al., 2022; Chen et al., 2018; Hezel et al., 2011; Spracklen et al., 2005). Our F_{DMS} is higher than the 18 Tg S yr^{-1} which uses sea surface DMS concentration from Kettle et al. (1999) as reported (Chen et al., 2018) indicating the DMS emission varies with change in sea surface DMS climatology. The analysis and improvement of DMS emissions directly is not a part of this work, but we note that improved and validated inventories for DMS will certainly play a role in subsequent oxidation product comparisons. We recommend ongoing evaluation of DMS emissions inputs to complement the expanded chemical mechanism development we present here.

In the BASE simulation the chemical loss of DMS acts as its only sink (as opposed to dry and wet deposition), leading to a full conversion yield of DMS into SO_2 (82.5%) and MSA (17.5%) (Fig. A3a). Figure 6 shows that in simulation MOD with updated DMS oxidation scheme DMS is mainly oxidized by OH in the gas phase, with 33.5% of losses proceeding via the H-abstraction channel and 29.4% via the OH-addition pathway, together contributing up to 62% of global average loss with high regional contribution over the tropical oceans via the abstraction channel where surface OH is the highest. NO_3 oxidation of DMS accounts for another 12.8% of global DMS chemical losses, comparable to values found in previous studies (Chen et al., 2018; Fung et al., 2022). Over the ocean, the NO_3 loss pathway is strongest in the NH coastal regions due to outflow of NO_x sources from over the land whereas for the SH values are generally less than 10%. Oxidation by BrO is responsible for 19.6% of the global DMS removal, falling within the previously estimated range of 8%–29% (Boucher et al., 2003; Khan et al., 2016; Chen et al., 2018). Regionally, its contribution can reach 50%–60% over high latitudes of the Southern Hemisphere as well as to the north near the Arctic Ocean, consistent with previous box model studies based on the availability of high BrO and low OH and NO_3 for those regions (Hoffmann et al., 2016). DMS + O_3 accounts for 2.7% (aqueous) and 1.1% (gas phase) of global surface DMS loss. The higher contribution from BrO and lower from O_3 using this mechanism compared to some previous studies could be explained in part by the recently implemented sea-salt debromination mechanism in GEOS-Chem, resulting in a much higher background level of BrO as well as lower O_3 abundance, especially in the southern hemisphere (Boucher et al., 2003; Chen et al., 2018; Fung et al., 2022; Sherwen et al., 2016a; Wang et al., 2021). To further quantify the importance of the sea salt debromination mechanism, we perform an emissions sensitivity test by turning this emission source off while using updated MOD chemistry (Fig. A1). As would be expected, these simulations show much lower BrO formation (as shown in Fig. A6) and resulting chemical impacts, with overall oxidation contributions comparable to previous literature (Schmidt et al., 2016; Wang et al., 2021). We find that under this scenario the relative contribution of BrO for DMS loss decreases to 3.8%, while the DMS + O_3 pathway increases to 4.0% (aqueous) and 1.8% (gas phase), and the DMS + OH pathway increases to 38.0% (abstraction) and 36.1% (addition) of global surface DMS loss (Fig. A1). The DMS loss via interaction with NO_3 also increases by 2.5% when sea salt debromination is turned off in the mechanism. The relative contributions of other oxidants remain mostly unaffected in the BrO sensitivity test.

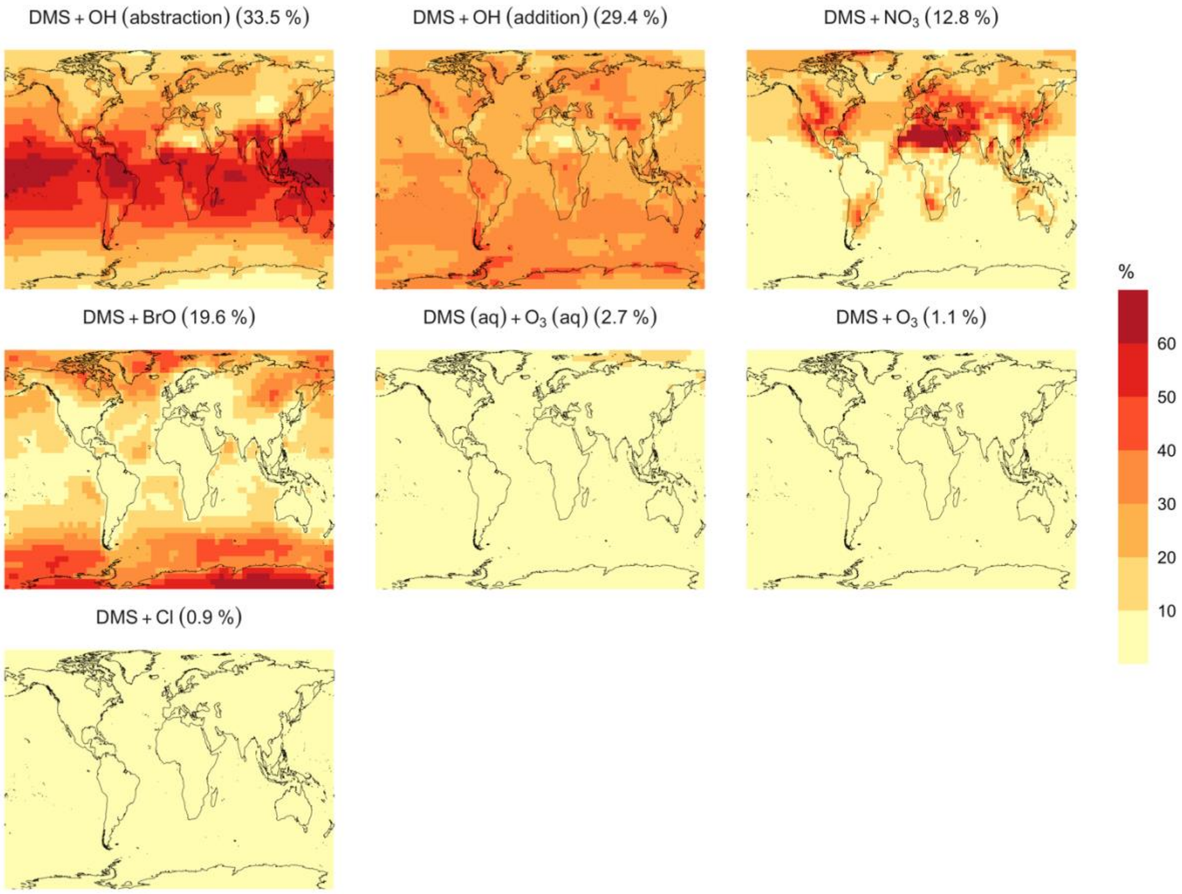

Figure 6 Geographic distribution of the annual mean surface layer fraction of total DMS oxidation (percent) attributed to different tropospheric oxidants for simulation MOD (described in Table 5). Percentages in parentheses indicates average contribution to global chemical loss for fraction of DMS emitted for each reaction pathways presented here.

Regionally, the fractional contribution of aqueous-phase DMS + O_3 to DMS oxidation can be up to 10%–20% over high-latitude oceans, which is in the middle of the 5%–30% contribution to high-latitude DMS losses previously reported (Chen et al., 2018; Fung et al., 2022; von Glasow and Crutzen, 2004). The Cl oxidation reaction contribute about 0.9% and 1.0% respectively for with and without sea salt debromination to the chemical removal of DMS, consistent with some previous studies (Atkinson et al., 2004; Fung et al., 2022). This does differ from other reported values however, including those from a global model study (4%) and box model simulations (8%–18%) (Chen et al., 2018; Hoffmann et al., 2016; von Glasow and Crutzen, 2004). It's worth noting that none of the studies reporting such high Cl contributions included HPMTF formation and loss. Ongoing uncertainties associated with model-observation bias of Cl should be further resolved to get better representation of halogenated species contributions to DMS loss (Wang et al., 2021). Due to slower reaction kinetics and lower fractional contribution reported earlier compared to BrO with DMS and uncertainty in surface concentration and kinetics for photochemically generated halogenated species such as Br, IO we did not include them in our chemical scheme (Chen et al., 2018).

3.3 Implications of the extended DMS oxidation mechanism

Figure 7 shows that the MOD simulation results in 35% reduction of surface layer SO_2 relative to BASE, but a huge increase in SO_4^{2-} in most regions. These changes suggest that the combination of gas-phase and aqueous-phase reactions results in a higher net yield of MSA and HPMTF and a lower net yield of gas-phase SO_2. Additionally, comparison of simulation MOD relative to MOD_noHetLossHPMTF (Fig. A2a) shows that loss of HPMTF in cloud droplets and aerosol reduces the global mean production of SO_2 by 19.6%, contributing to the SO_2 reduction and increasing mean surface layer sulfate by 16.1% (Fig. A2b). This reduction in SO_2 is expected to reduce the availability of gas-phase sulfuric acid for new particle formation by nucleation (Clarke et al., 1998a). Total SO_4^{2-} increases over the ocean, however, because the increased SO_4^{2-} production from rapid loss of MSA and HPMTF in aqueous-phase offsets the reduced oxidation of SO_2 (Fig. 7b).

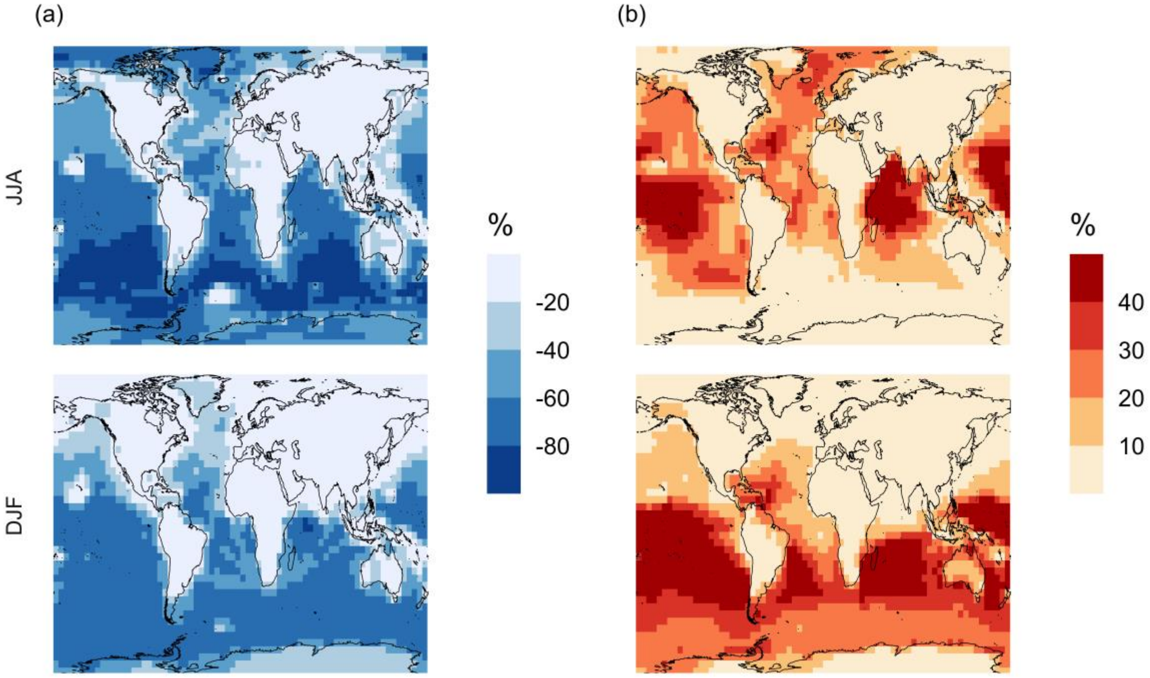

Figure 7 Percent change in simulated surface layer (a) SO_2 and (b) SO_4^{2-} for simulation MOD relative to BASE for June, July and August mean (JJA) and December, January, and February mean (DJF). Simulations are described in Table 5.

Qualitatively, the regions showing the highest percent changes of SO_2 are consistent with previous studies that included HPMTF chemistry and loss processes though the extent of this reduction is much higher with the integrated mechanism used in our study (Fig. 7a) (Novak et al., 2021). The regions with the largest percent change in SO_2 reduction are those where DMS oxidation contributes most to SO_2, and where HPMTF production and in-cloud oxidation of HPMTF are efficient. This spatial pattern thus helps us to identify where the production and heterogeneous loss of HPMTF and MSA is enhanced. One of the reactions that possibly contributes to delayed formation and reduction of SO_2 concentration is the first-generation OCS formation from OH oxidation of HPMTF. We find that addition of cloud and aerosol loss significantly decreases the OCS production, especially in high cloud cover regions as previously reported (Jernigan et al., 2022a). Even though the cloud loss of HPMTF increases the production of surface sulfate, the total global sulfate burden we calculate increases by only 4.1% from the BASE sulfate burden of around 575 Gg S. This can be attributed to minor contribution of DMS and its intermediate oxidation products in SO_2 production compared to other non-DMS derived sources. In addition, the production of stable intermediate oxidation products delay the conversion of SO_2 to SO_4^{2-} and modify its spatial distribution in the marine environment. Thus, we should expect these aqueous phase oxidation products to contribute to particle mass rather than increase the number of nucleated particles, as suggested in other studies (Clarke et al., 1998b; Novak et al., 2021; Williamson et al., 2019).

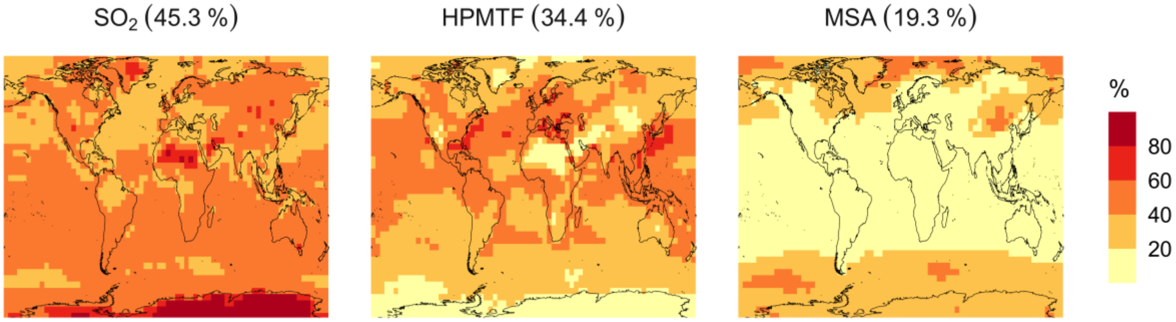

Figure 8 Simulated branching ratio (in %) of the DMS oxidation mechanism considering SO_2, HPMTF and MSA as major terminal oxidation products calculated from their annual total production rate for simulation MOD.

The spatial distribution of product branching ratios of DMS oxidation is shown in Figure 8. Here, 34.4% of the annual total DMS oxidation will end up as HPMTF, while final SO_2 yield decreases to 45.3% compared to 82.5% for the BASE simulation (Fig. A3a). The terminal HPMTF branch represents sulfur removed from the system by cloud and aerosol uptake of HPMTF, leading to a reduced overall formation of SO_2. With sea salt debromination turned off, modified chemistry forms even more HPMTF (41.7%), slightly higher SO_2 (46.4%), and lowers the yield of MSA to 11.9% (19.3% with the sea salt debromination on), underscoring the importance of halogen chemistry for MSA production (Fig. A3b). These results are broadly consistent with observationally constrained estimates from ATom-4 flight campaigns, where ~ 30% - 40% DMS was oxidized to HPMTF along their flight tracks compared to 34.4% for the full branch of HPMTF in the present work, as well as with previous modeling studies showing 33% HPMTF formation as terminating product (Veres et al., 2020; Fung et al., 2022). MSA is produced mostly by aqueous phase oxidation of MSIA by O_3 and OH according to the mechanism used here and has high abundance near the Southern Ocean and Antarctic belt as reported by previous studies (Chen et al., 2018; Hoffmann et al., 2016; Fung et al., 2022). The global burden of MSA decreases dramatically, from 19 Gg S for 'Base' to 8.5 Gg S for simulation MOD. The higher rate of major loss process or lower rate of production of MSA from the aqueous phase reactions could be responsible for this reduction in global budget (Fung et al., 2022).

3.4 Impact on aerosol size distributions

Following the percent change in simulated surface layer SO_2 and SO_4^{2-} for modified DMS chemistry (Fig. 7), we further explore how this expanded DMS oxidation chemistry impacts modeled aerosol size distributions. Figure 9 shows the global mean surface-layer percent change in the normalized aerosol number concentration for modified chemistry relative to the BASE simulation, with and without cloud and aerosol HPMTF loss processes. The aerosol number concentration decreases for the sub-80 nm diameter size bins for both simulations, especially during the DJF months when cloud and aerosol loss pathways of HPMTF are included (MOD case), demonstrating the negative impact of these processes on simulated new particle formation. Without these processes included (as in case MOD_noHetLossHPMTF), percent changes are far more modest for these smaller size ranges. On the other hand, HPMTF lost to clouds and aerosols increases the simulated number of particles with diameter above 100 nm in the MOD simulation, consistent with the increase in sulfate mass concentrations shown in Fig. 7 and suggesting that HPMTF heterogenous loss promotes simulated particle growth to diameters larger than 80-100 nm. The greater abundance of particles larger than 100 nm also acts as a condensation sink, further suppressing nucleation and growth at smaller size ranges.

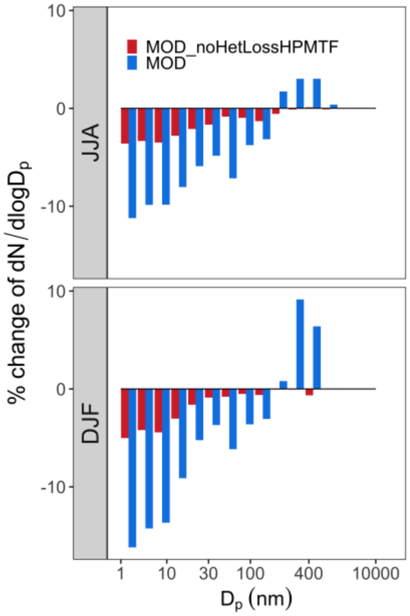

Figure 9 Global mean surface-layer percent change in normalized aerosol number concentration for different size bins with particle diameter, D_p in the range of 3 nm < D_p < 10000 nm for simulations MOD and MOD_noHetLossHPMTF relative to simulation BASE. Simulations are described in Table 5.

The geographic distribution of surface layer aerosol number concentration for aerosol in the size range of 3 – 80 nm for two seasons is shown in Figure 10. We find that global mean aerosol number concentration in this size range decreases for simulations MOD and MOD_noHetLossHPMTF relative to BASE by 12.8% and 9.9% respectively. Decreases are greater for simulation MOD (Fig. 10b). Fig. 10c shows the effect of HPMTF heterogenous loss processes on the number of particles with diameters between 3-80 nm for simulation MOD relative to simulation MOD_noHetLossHPMTF. The largely negative impact of HPMTF loss to clouds and aerosols on sub-80 nm particle number is contributed to by enhanced direct sulfate formation on pre-existing particles, bypassing gas-phase SO_2 formation (a precursor for new particle formation). As well, in the model, new particles grow through condensation of H_2SO_4 and organics and their growth are dependent on the condensation sink, while loss of particle number depends on the coagulation sink. Thus, changes to the condensation/coagulation sinks and sulfuric acid production rate through the updated mechanism will also alter the growth rates of small particles (sub-80 nm) as well as their coagulation loss rates. Hence, similar to the discussion for Figure 9, the reduction of gas-phase production of H_2SO_4 in MOD relative to BASE slows new-particle formation and growth, while the additional production of sulfate through aqueous chemistry on larger particles in MOD increases the coagulational scavenging of the newly formed particles. These two effects synergistically reduce the concentration of ultrafine particles in the model. The fraction of newly formed particles that can reach the CCN size is dependent on the particle growth rates, especially for particle sizes below 10 nm, where we see highest coagulation losses to larger particles. The sensitivity of these results to the new sea salt debromination parameterization is shown in Fig. A4, where we find a regional increase in aerosol number concentration at mid to higher latitude of the SH despite low BrO concentrations (Fig A4).

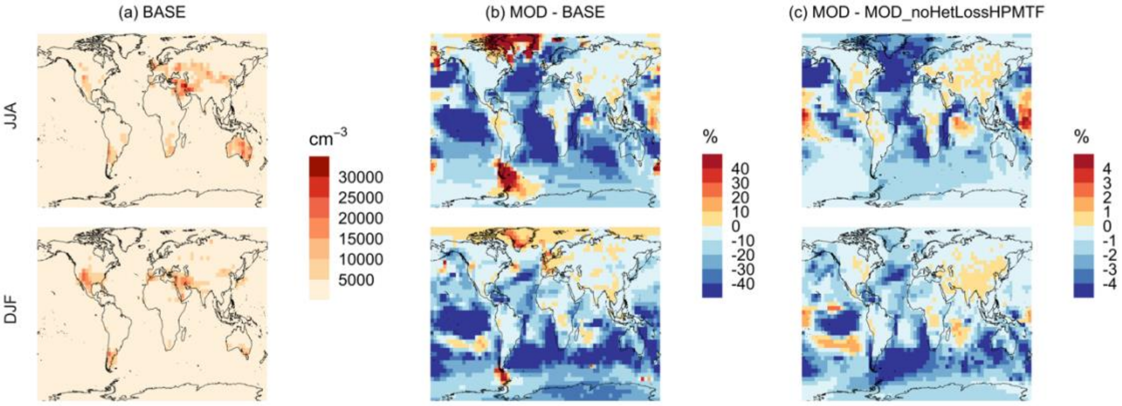

Figure 10 Geographic distribution of seasonal-mean surface-layer aerosol number concentration in cm^{-3} (for particles with diameters between 3 – 80 nm) for (a) the BASE simulation, (b) the percent difference between MOD and BASE and (c) the percent difference between MOD and MOD_noHetLossHPMTF to show the role of cloud and aerosol loss of HPMTF. Simulations are described in Table 5.

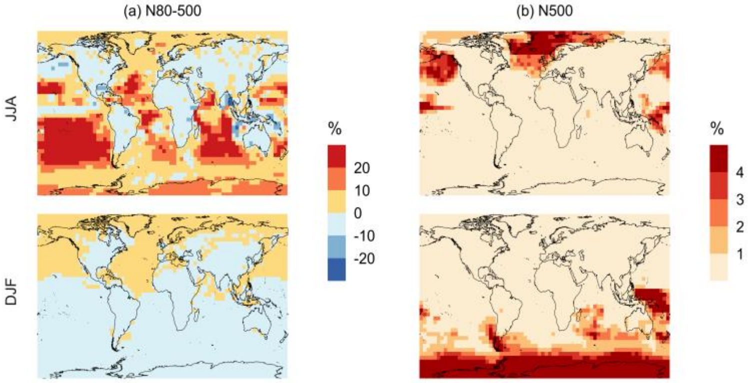

Figure 11 Geographic distribution of percent difference in seasonal-mean surface-layer aerosol number concentration in cm^{-3} for simulations MOD relative to simulations BASE for diameters between (a) 80 – 500 nm and (b) >500 nm. Simulations are described in Table 5.

Finally, we also analyze the impact of this expanded DMS scheme on particles larger than 80 nm (Fig. 11). We find increases of around 6.6% for JJA mean surface layer number concentration of aerosol with diameters between 80-500 nm, while DJF months show mean reductions of -5.4% for DJF despite largely positive changes in the marine NH for these months (Fig. 11a). However, for the > 500 nm size ranges (Fig. 11b), the global mean surface layer number concentration of aerosol mostly increases, with highest changes occurring in the areas of peak DMS emission in both hemispheres, during their summertime season. A similar trend is observed in the absence of cloud and aerosol HPMTF uptake in simulation MOD_noHetLossHPMTF (Fig. A5).

Comparing the regional extent and direction of this change, we find the net increase in particle number concentration is higher for MOD compared to MOD_noHetLossHPMTF, highlighting the importance of HPMTF loss processes to clouds and aerosols as a contributor of CCN.

4 Conclusion

In this study we update the default DMS oxidation scheme in the GEOS-Chem model by implementing an integrated oxidation mechanism. The new scheme includes gas-phase and aqueous phase reactions involving DMSO, MSIA and HPMTF formation, as well as newly identified HPMTF loss processes yielding considerable changes in seasonal concentrations of major oxidation products and sulfur-derived aerosols. With this new chemistry scheme, global annual mean surface DMS concentration decreases by 38% relative to the BASE scheme in GEOS-Chem globally due to the presence of additional loss processes in the integrated mechanism reducing the bias to ATom-4 DMS measurement.

In this new scheme, OH, BrO, O_3 and NO_x species act as important sinks of DMS contributing to 62.9%, 19.6%, 3.8% and 12.8% global annual mean surface DMS loss, highlighting the relative importance of these loss process in determining surface DMS budget. We also find that at higher latitudes, gas phase and multiphase oxidation of DMS by O_3 and BrO becomes important to determine the budget of DMS. On the other hand, at lower latitudes OH contribute to a greater extent compared to other sinks and at comparable extent to previous studies exploring this chemistry. For the global distribution of simulated HPMTF, our updated scheme in GEOS-Chem provides a reduced high bias against observations compared to previous studies. While emissions of BrO are uncertain in this version of GEOS-Chem, we find that the compound acts as a key sink of DMS, especially over the Southern Ocean. Overall, we find large reduction in SO_2 (35%) and an increase in sulfate (22%) due to the addition of heterogeneous HPMTF loss processes.

The lower SO_2 with the new DMS chemistry scheme contributes to a reduction in the global annual mean surface layer number concentration of particles with diameters less than 80 nm by 12.8%, contributed to by reductions in gas-phase precursors for new particle formation. There is a concurrent increase of 3.1% in the global annual mean number of particles with diameters larger than 80 nm. This latter global mean particle number change varies in sign seasonally, with a 6.6% increase for JJA, and a 5.4% decrease for DJF. This decrease is dominated by southern hemisphere summertime changes, connected with suppressed new particle formation/growth and enhanced coagulation following additional sulfate production through aqueous chemistry. Cloud loss processes related to HPMTF make key contributions to these simulated changes through enhancement of aqueous-phase particle growth of those particle large enough to act as CCN.

Although the increased chemical mechanism complexity described in this work will necessarily increase model computational cost (MOD simulation run times increase by approximately 16%), this study highlights the value of including a more realistic chemical oxidation mechanism of DMS and its stable intermediates for better representation of DMS-derived aerosol in the marine atmosphere, as well as its seasonal size distributions. A reduced form of the key chemical species and pathways should be able to capture the key processes with less computational impact and will be a priority in future work.

Appendix A: Additional figures

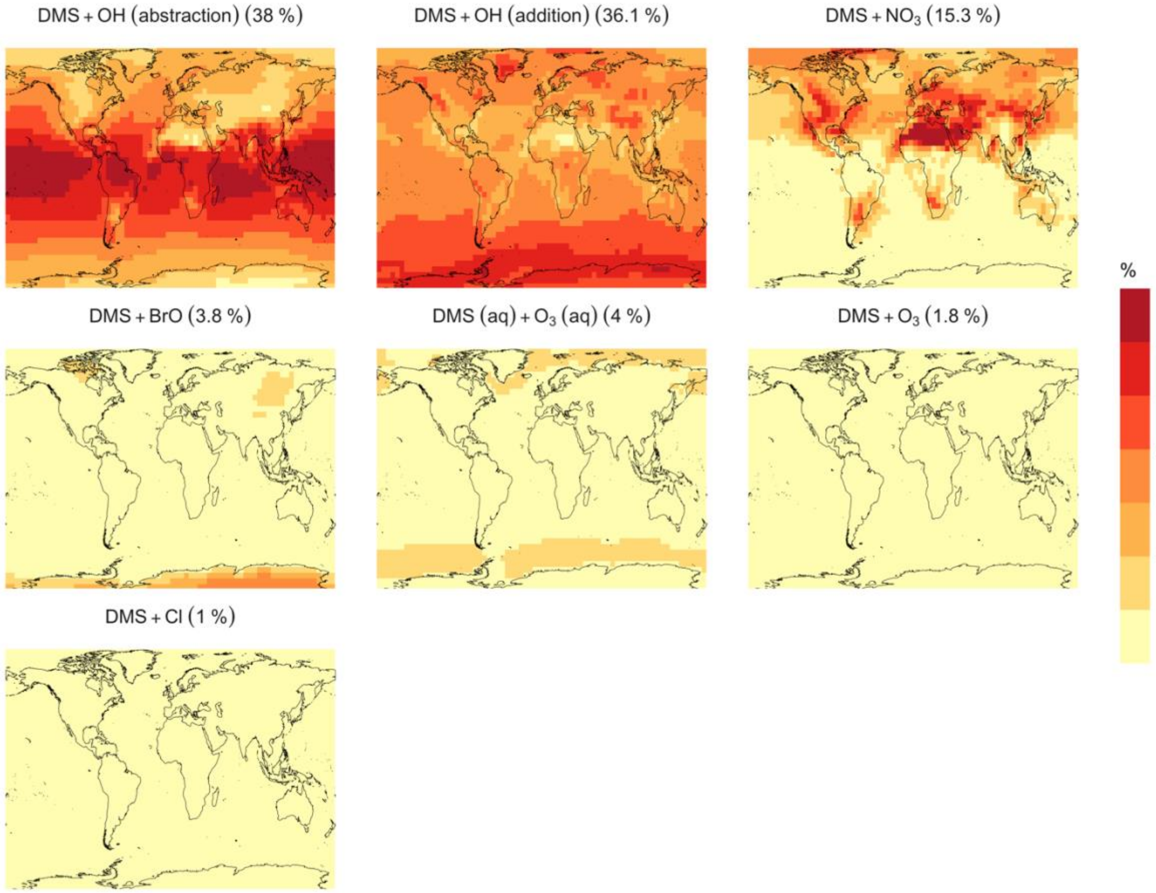

Figure A1 Surface layer geographic distribution of the simulated annual mean fraction of total DMS oxidation (percent) attributed to different tropospheric oxidants for a simulation otherwise the same as simulation MOD except with no sea salt debromination. Percentages in parentheses indicates average contribution to global chemical loss as a fraction of DMS emitted for each reaction pathways presented here. Simulations are described in Table 5.

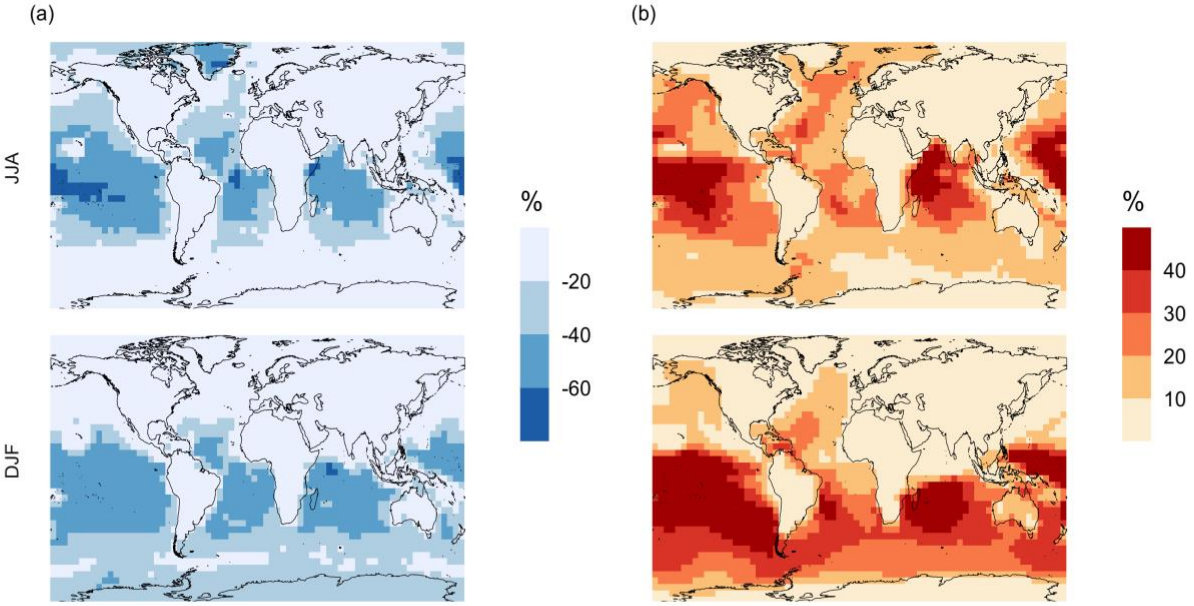

Figure A2 Percent change in simulated surface layer (a) SO_2 and (b) SO_4^{2-} for simulation MOD relative to MOD_noHetLossHPMTF for June, July and August mean (JJA) and December, January, and February mean (DJF). Simulations are described in Table 5.

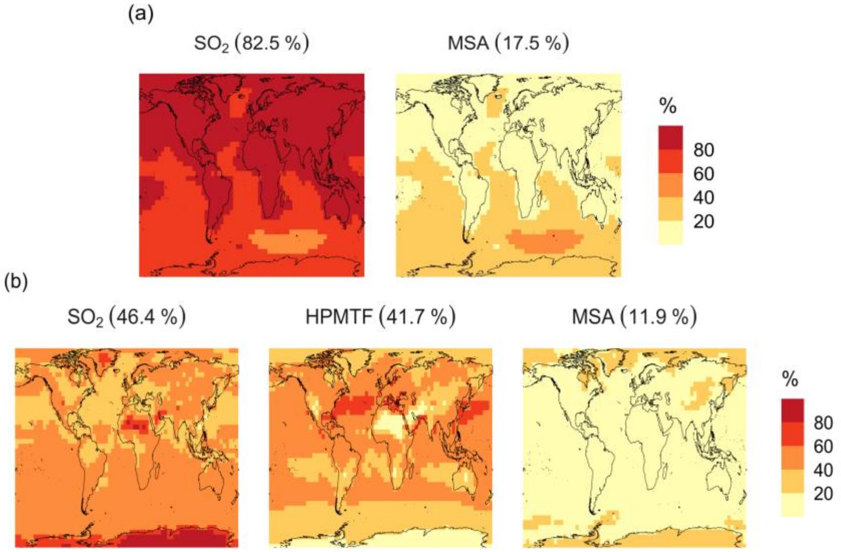

Figure A3 Simulated annual mean surface layer branching ratios (in %) of the DMS oxidation mechanism considering SO_2, HPMTF, and MSA as major oxidation products calculated from their total production rates for simulations similar to (a, top row) BASE and (b, bottom row) MOD, except all with no sea salt debromination. Simulations are described in Table 5.

595

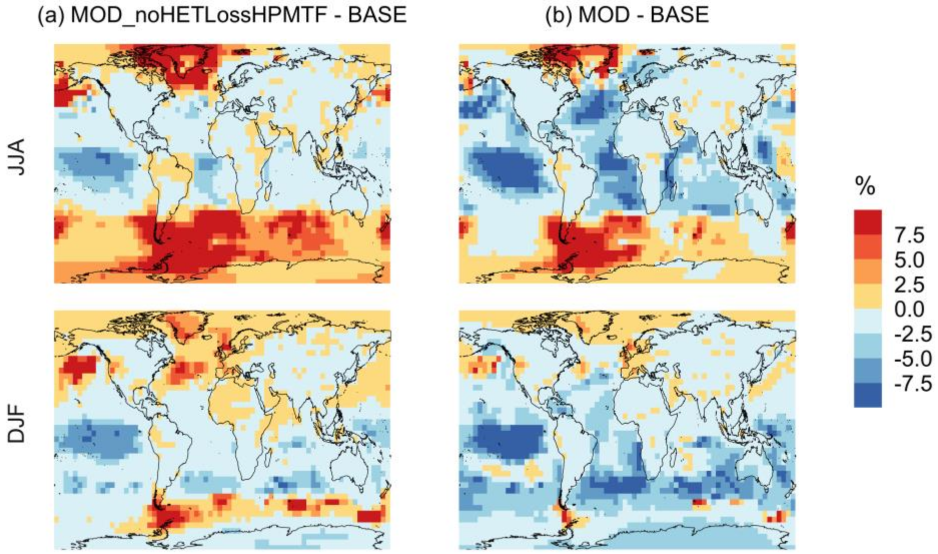

Figure A4 Geographic distribution of percent difference in seasonal-mean surface-layer aerosol number concentration in cm-3 (for particles with diameters between 3 – 80 nm) for simulations similar to (a) MOD_noHetLossHPMTF and (b) MOD relative to simulations BASE, except all with no sea salt debromination. Simulations are described in Table 5.

596

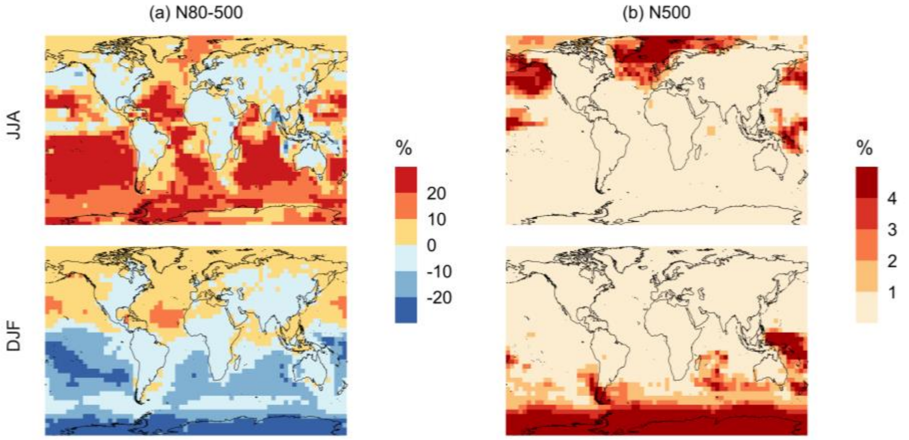

Figure A5 Geographic distribution of percent difference in seasonal-mean surface-layer aerosol number concentration in cm-3 for simulations similar to MOD_noHetLossHPMTF relative to simulations BASE, for particle diameters between (a) 80 – 500 nm and (b) > 500 nm. Simulations are described in Table 5.

597

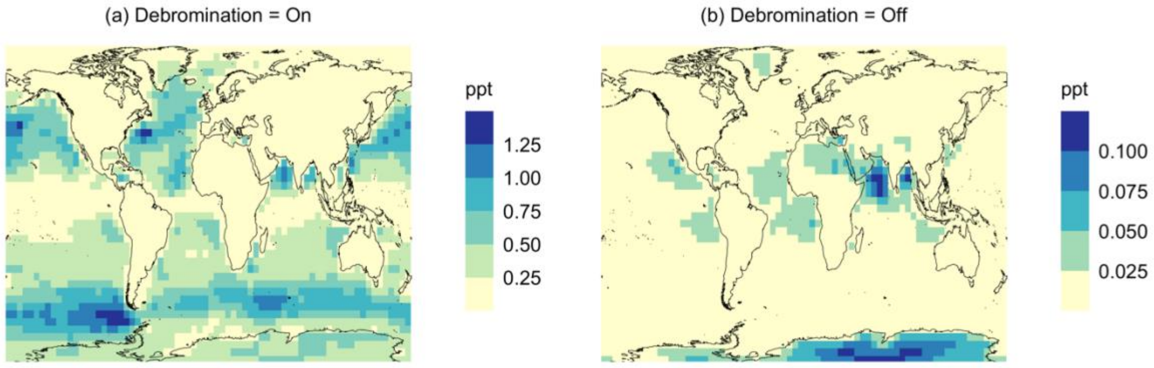

Figure A6 Geographic distribution of mean surface BrO mixing ratio (ppt) for (a) with sea salt debromination and (b) without sea salt debromination for simulation MOD. Simulations are described in Table 5.

Appendix B: Additional Table

Table B1. Global atmospheric flux, deposition, burdens, lifetime of DMS and its oxidation products, chemical loss rates for specific reaction pathways and global mean concentration of major oxidants are listed here for the case of simulation MOD. Note that SO_2 and SO_4^{2-} includes natural as well as anthropogenic sources.

F_{DMS} (Gg S yr^{-1})	2.2 x 10^4
Deposition of MSA (Gg S yr^{-1})	3.6 x 10^3
Deposition of HPMTF (Gg S yr^{-1})	9.1 x 10^1
Deposition of DMSO (Gg S yr^{-1})	1.7 x 10^3
Deposition of MSIA (Gg S yr^{-1})	2.2 x 10^2
DMS (GgS)	67
MSA (GgS)	8.5
HPMTF (GgS)	0.75
SO_2 (GgS)	261.5
SO_4^{2-} (GgS)	598.6
τ_{DMS} (d)	1.0
τ_{MSA} (d)	0.8
τ_{HPMTF} (d)	0.7
τ_{SO2} (d)	1.3
$\tau_{SO4}{}^{2-}$ (d)	4.4
DMS lost to MSA (Gg S yr^{-1})	4.1 x 10^3
DMS lost to HPMTF (Gg S yr^{-1})	7.6 x 10^3
DMS lost to SO_2 (Gg S yr^{-1})	9.2 x 10^3
MSA lost to particle growth (Gg S yr^{-1})	4.3 x 10^2
HPMTF lost to SO_2 (Gg S yr^{-1})	4.5 x 10^2
HPMTF lost to cloud (Gg S yr^{-1})	6.7 x 10^3
HPMTF lost to particle growth (Gg S yr^{-1})	2.7 x 10^2
OH (molec cm^{-3})	1.1 x 10^6
Cl (molec cm^{-3})	4.5 x 10^7
NO_3 (molec cm^{-3})	2.0 x 10^{12}
O_3 (molec cm^{-3})	4.4x 10^{16}
BrO (molec cm^{-3})	6.3 x 10^{11}

Data availability. The DMS observational data in Fig. 2 were obtained from the referenced papers (Kouvarakis and Mihalopoulos, 2002; Castebrunet et al., 2009). The observations data during ATom-4 are published through the Distributed Active Archive Center for Biogeochemical Dynamics (DAAC) at (Novak et al., 2021; Wollesen de Jonge et al., 2021), https://doi.org/10.3334/ORNLDAAC/1921 and https://daac.ornl.gov/ATOM/guides/ATom_SO2_LIF_Instrument_Data.html.

Author contributions. LT and WCP designed the research goals, aims, and methodology, implemented the new code into GC-TOMAS. QC, BA, CHF and CDH contributed in code development. All authors provided expert advice on data analysis, interpretation, and visualization. LT ran model simulations, analyzed the data, created the figures, and led manuscript development and editing.

Competing interests. The contact authors have declared that none of the authors has any competing interests.

Acknowledgements. LT and WCP gratefully acknowledge Ka Ming Fung for discussions on DMS oxidation chemistry. BC thanks Rachel Y.-W. Chang for discussions on marine aerosols.

Financial support. LT and WCP was supported by NSF grant no. 2155192. QC was supported by the Hong Kong Research Grants Council (Grant No. 15223221 and 15219722). BA was supported by NSF AGS 2109323 and PLR 1904128. CHF was supported by NASA FINESST (grant 80NSSC19K1368). CDH acknowledges funding support from NSF AGS (grant 1848372). BC gratefully acknowledges research funding supported by the Ocean Frontier Institute, through an award from the Canada First Research Excellence Fund. JRP was supported by the Atmospheric System Research (ASR) program, part of the US Department of Energy's Office of Biological and Environmental Research within the Office of Science, under grant DE-SC0021208. SI was supported by Ferring Pharmaceuticals through the Extreme Environments research Laboratory, École Polytechnique Fédérale de Lausanne (EPFL).

References

Adams, P. J. and Seinfeld, J. H.: Predicting global aerosol size distributions in general circulation models, J. Geophys. Res. Atmospheres, 107, AAC 4-1-AAC 4-23, https://doi.org/10.1029/2001JD001010, 2002.

Alexander, B., Park, R. J., Jacob, D. J., Li, Q. B., Yantosca, R. M., Savarino, J., Lee, C. C. W., and Thiemens, M. H.: Sulfate formation in sea-salt aerosols: Constraints from oxygen isotopes, J. Geophys. Res. Atmospheres, 110, https://doi.org/10.1029/2004JD005659, 2005.

Alexander, B., Park, R. J., Jacob, D. J., and Gong, S.: Transition metal-catalyzed oxidation of atmospheric sulfur: Global implications for the sulfur budget, J. Geophys. Res. Atmospheres, 114, https://doi.org/10.1029/2008JD010486, 2009.

Amos, H. M., Jacob, D. J., Holmes, C. D., Fisher, J. A., Wang, Q., Yantosca, R. M., Corbitt, E. S., Galarneau, E., Rutter, A. P., Gustin, M. S., Steffen, A., Schauer, J. J., Graydon, J. A., Louis, V. L. S., Talbot, R. W., Edgerton, E. S., Zhang, Y., and Sunderland, E. M.: Gas-particle partitioning of atmospheric Hg(II) and its effect on global mercury deposition, Atmospheric Chem. Phys., 12, 591–603, https://doi.org/10.5194/acp-12-591-2012, 2012.

Atkinson, R., Baulch, D. L., Cox, R. A., Crowley, J. N., Hampson, R. F., Hynes, R. G., Jenkin, M. E., Rossi, M. J., and Troe, J.: Evaluated kinetic and photochemical data for atmospheric chemistry: Volume I - gas phase reactions of O_x, HO_x, NO_x and SO_x species, Atmospheric Chem. Phys., 4, 1461–1738, https://doi.org/10.5194/acp-4-1461-2004, 2004.

Bardouki, H., da Rosa, M. B., Mihalopoulos, N., Palm, W.-U., and Zetzsch, C.: Kinetics and mechanism of the oxidation of dimethylsulfoxide (DMSO) and methanesulfinate (MSI−) by OH radicals in aqueous medium, Atmos. Environ., 36, 4627–4634, https://doi.org/10.1016/S1352-2310(02)00460-0, 2002.

Barnes, I., Hjorth, J., and Mihalopoulos, N.: Dimethyl Sulfide and Dimethyl Sulfoxide and Their Oxidation in the Atmosphere, Chem. Rev., 106, 940–975, https://doi.org/10.1021/cr020529+, 2006.

Berndt, T., Scholz, W., Mentler, B., Fischer, L., Hoffmann, E. H., Tilgner, A., Hyttinen, N., Prisle, N. L., Hansel, A., and Herrmann, H.: Fast Peroxy Radical Isomerization and OH Recycling in the Reaction of OH Radicals with Dimethyl Sulfide, J. Phys. Chem. Lett., 10, 6478–6483, https://doi.org/10.1021/acs.jpclett.9b02567, 2019.

Berndt, T., Hoffmann, E. H., Tilgner, A., Stratmann, F., and Herrmann, H.: Direct sulfuric acid formation from the gas-phase oxidation of reduced-sulfur compounds, Nat. Commun., 14, 4849, https://doi.org/10.1038/s41467-023-40586-2, 2023.

Bey, I., Jacob, D. J., Yantosca, R. M., Logan, J. A., Field, B. D., Fiore, A. M., Li, Q., Liu, H. Y., Mickley, L. J., and Schultz, M. G.: Global modeling of tropospheric chemistry with assimilated meteorology: Model description and evaluation, J. Geophys. Res. Atmospheres, 106, 23073–23095, https://doi.org/10.1029/2001JD000807, 2001.

Boniface, J., Shi, Q., Li, Y. Q., Cheung, J. L., Rattigan, O. V., Davidovits, P., Worsnop, D. R., Jayne, J. T., and Kolb, C. E.: Uptake of Gas-Phase SO2, H2S, and CO2 by Aqueous Solutions, J. Phys. Chem. A, 104, 7502–7510, https://doi.org/10.1021/jp000479h, 2000.

Boucher, O., Moulin, C., Belviso, S., Aumont, O., Bopp, L., Cosme, E., von Kuhlmann, R., Lawrence, M. G., Pham, M., Reddy, M. S., Sciare, J., and Venkataraman, C.: DMS atmospheric concentrations and sulphate aerosol indirect radiative forcing: a sensitivity study to the DMS source representation and oxidation, Atmospheric Chem. Phys., 3, 49–65, https://doi.org/10.5194/acp-3-49-2003, 2003.

Bräuer, P., Tilgner, A., Wolke, R., and Herrmann, H.: Mechanism development and modelling of tropospheric multiphase halogen chemistry: The CAPRAM Halogen Module 2.0 (HM2), J. Atmospheric Chem., 70, 19–52, https://doi.org/10.1007/s10874-013-9249-6, 2013.

Breider, T. J., Chipperfield, M. P., Richards, N. a. D., Carslaw, K. S., Mann, G. W., and Spracklen, D. V.: Impact of BrO on dimethylsulfide in the remote marine boundary layer, Geophys. Res. Lett., 37, https://doi.org/10.1029/2009GL040868, 2010.

Burkholder, J. B., Sander, S. P., Abbatt, J. P. D., Barker, J. R., Huie, R. E., Kolb, C. E., Kurylo, M. J., Orkin, V. L., Wilmouth, D. M., and Wine, P. H.: Chemical kinetics and photochemical data for use in atmospheric studies: evaluation number 18, 2015.

Burkholder, J. B., Sander, S. P., Abbatt, J. P. D., Barker, J. R., Cappa, C., Crounse, J. D., Dibble, T. S., Huie, R. E., Kolb, C. E., Kurylo, M. J., Orkin, V. L., Percival, C. J., Wilmouth, D. M., and Wine, P. H.: Chemical kinetics and photochemical data for use in atmospheric studies; evaluation number 19, 2020.

Carslaw, K. S., Lee, L. A., Reddington, C. L., Pringle, K. J., Rap, A., Forster, P. M., Mann, G. W., Spracklen, D. V., Woodhouse, M. T., Regayre, L. A., and Pierce, J. R.: Large contribution of natural aerosols to uncertainty in indirect forcing, Nature, 503, 67–71, https://doi.org/10.1038/nature12674, 2013.

Castebrunet, H., Martinerie, P., Genthon, C., and Cosme, E.: A three-dimensional model study of methanesulphonic acid to non sea salt sulphate ratio at mid and high-southern latitudes, Atmospheric Chem. Phys., 9, 9449–9469, https://doi.org/10.5194/acp-9-9449-2009, 2009.

Charlson, R. J., Lovelock, J. E., Andreae, M. O., and Warren, S. G.: Oceanic phytoplankton, atmospheric sulphur, cloud albedo and climate, Nature, 326, 655–661, https://doi.org/10.1038/326655a0, 1987.

Chen, H., Ezell, M. J., Arquero, K. D., Varner, M. E., Dawson, M. L., Gerber, R. B., and Finlayson-Pitts, B. J.: New particle formation and growth from methanesulfonic acid, trimethylamine and water, Phys. Chem. Chem. Phys., 17, 13699–13709, https://doi.org/10.1039/C5CP00838G, 2015.

Chen, Q., Geng, L., Schmidt, J. A., Xie, Z., Kang, H., Dachs, J., Cole-Dai, J., Schauer, A. J., Camp, M. G., and Alexander, B.: Isotopic constraints on the role of hypohalous acids in sulfate aerosol formation in the remote marine boundary layer, Atmospheric Chem. Phys., 16, 11433–11450, https://doi.org/10.5194/acp-16-11433-2016, 2016.

Chen, Q., Schmidt, J. A., Shah, V., Jaeglé, L., Sherwen, T., and Alexander, B.: Sulfate production by reactive bromine: Implications for the global sulfur and reactive bromine budgets, Geophys. Res. Lett., 44, 7069–7078, https://doi.org/10.1002/2017GL073812, 2017.

Chen, Q., Sherwen, T., Evans, M., and Alexander, B.: DMS oxidation and sulfur aerosol formation in the marine troposphere: a focus on reactive halogen and multiphase chemistry, Atmospheric Chem. Phys., 18, 13617–13637, https://doi.org/10.5194/acp-18-13617-2018, 2018.

Chin, M., Jacob, D. J., Gardner, G. M., Foreman-Fowler, M. S., Spiro, P. A., and Savoie, D. L.: A global three-dimensional model of tropospheric sulfate, J. Geophys. Res. Atmospheres, 101, 18667–18690, https://doi.org/10.1029/96JD01221, 1996.

Clarke, A. D., Davis, D., Kapustin, V. N., Eisele, F., Chen, G., Paluch, I., Lenschow, D., Bandy, A. R., Thornton, D., Moore, K., Mauldin, L., Tanner, D., Litchy, M., Carroll, M. A., Collins, J., and Albercook, G.: Particle Nucleation in the Tropical Boundary Layer and Its Coupling to Marine Sulfur Sources, Science, 282, 89–92, 1998a.

Clarke, A. D., Varner, J. L., Eisele, F., Mauldin, R. L., Tanner, D., and Litchy, M.: Particle production in the remote marine atmosphere: Cloud outflow and subsidence during ACE 1, J. Geophys. Res. Atmospheres, 103, 16397–16409, https://doi.org/10.1029/97JD02987, 1998b.

Du, L., Xu, Y., Ge, M., Jia, L., Yao, L., and Wang, W.: Rate constant of the gas phase reaction of dimethyl sulfide (CH3SCH3) with ozone, Chem. Phys. Lett., 436, 36–40, https://doi.org/10.1016/j.cplett.2007.01.025, 2007.

Duncan Fairlie, T., Jacob, D. J., and Park, R. J.: The impact of transpacific transport of mineral dust in the United States, Atmos. Environ., 41, 1251–1266, https://doi.org/10.1016/j.atmosenv.2006.09.048, 2007.

Emerson, E. W., Hodshire, A. L., DeBolt, H. M., Bilsback, K. R., Pierce, J. R., McMeeking, G. R., and Farmer, D. K.: Revisiting particle dry deposition and its role in radiative effect estimates, Proc. Natl. Acad. Sci., 117, 26076–26082, https://doi.org/10.1073/pnas.2014761117, 2020.

Enami, S., Nakano, Y., Hashimoto, S., Kawasaki, M., Aloisio, S., and Francisco, J. S.: Reactions of Cl Atoms with Dimethyl Sulfide: A Theoretical Calculation and an Experimental Study with Cavity Ring-Down Spectroscopy, J. Phys. Chem. A, 108, 7785–7789, https://doi.org/10.1021/jp049772y, 2004.

Faloona, I.: Sulfur processing in the marine atmospheric boundary layer: A review and critical assessment of modeling uncertainties, Atmos. Environ., 43, 2841–2854, https://doi.org/10.1016/j.atmosenv.2009.02.043, 2009.

Flyunt, R., Makogon, O., Schuchmann, M. N., Asmus, K.-D., and Sonntag, C. von: OH-Radical-induced oxidation of methanesulfinic acid. The reactions of the methanesulfonyl radical in the absence and presence of dioxygen, J. Chem. Soc. Perkin Trans. 2, 787–792, https://doi.org/10.1039/B009631H, 2001.

Fung, K. M., Heald, C. L., Kroll, J. H., Wang, S., Jo, D. S., Gettelman, A., Lu, Z., Liu, X., Zaveri, R. A., Apel, E. C., Blake, D. R., Jimenez, J.-L., Campuzano-Jost, P., Veres, P. R., Bates, T. S., Shilling, J. E., and Zawadowicz, M.: Exploring dimethyl sulfide (DMS) oxidation and implications for global aerosol radiative forcing, Atmospheric Chem. Phys., 22, 1549–1573, https://doi.org/10.5194/acp-22-1549-2022, 2022.

Galí, M., Levasseur, M., Devred, E., Simó, R., and Babin, M.: Sea-surface dimethylsulfide (DMS) concentration from satellite data at global and regional scales, Biogeosciences, 15, 3497–3519, https://doi.org/10.5194/bg-15-3497-2018, 2018.

Galí, M., Devred, E., Babin, M., and Levasseur, M.: Decadal increase in Arctic dimethylsulfide emission, Proc. Natl. Acad. Sci., 116, 19311–19317, https://doi.org/10.1073/pnas.1904378116, 2019.

Gershenzon, M., Davidovits, P., Jayne, J. T., Kolb, C. E., and Worsnop, D. R.: Simultaneous Uptake of DMS and Ozone on Water, J. Phys. Chem. A, 105, 7031–7036, https://doi.org/10.1021/jp010696y, 2001.

von Glasow, R. and Crutzen, P. J.: Model study of multiphase DMS oxidation with a focus on halogens, Atmospheric Chem. Phys., 4, 589–608, https://doi.org/10.5194/acp-4-589-2004, 2004.

Hezel, P. J., Alexander, B., Bitz, C. M., Steig, E. J., Holmes, C. D., Yang, X., and Sciare, J.: Modeled methanesulfonic acid (MSA) deposition in Antarctica and its relationship to sea ice, J. Geophys. Res. Atmospheres, 116, https://doi.org/10.1029/2011JD016383, 2011.

Hodshire, A. L., Campuzano-Jost, P., Kodros, J. K., Croft, B., Nault, B. A., Schroder, J. C., Jimenez, J. L., and Pierce, J. R.: The potential role of methanesulfonic acid (MSA) in aerosol formation and growth and the associated radiative forcings, Atmospheric Chem. Phys., 19, 3137–3160, https://doi.org/10.5194/acp-19-3137-2019, 2019.

Hoffmann, E. H., Tilgner, A., Schrödner, R., Bräuer, P., Wolke, R., and Herrmann, H.: An advanced modeling study on the impacts and atmospheric implications of multiphase dimethyl sulfide chemistry, Proc. Natl. Acad. Sci., 113, 11776–11781, https://doi.org/10.1073/pnas.1606320113, 2016.

Hoffmann, E. H., Heinold, B., Kubin, A., Tegen, I., and Herrmann, H.: The Importance of the Representation of DMS Oxidation in Global Chemistry-Climate Simulations, Geophys. Res. Lett., 48, e2021GL094068, https://doi.org/10.1029/2021GL094068, 2021.

Holmes, C. D., Bertram, T. H., Confer, K. L., Graham, K. A., Ronan, A. C., Wirks, C. K., and Shah, V.: The Role of Clouds in the Tropospheric NOx Cycle: A New Modeling Approach for Cloud Chemistry and Its Global Implications, Geophys. Res. Lett., 46, 4980–4990, https://doi.org/10.1029/2019GL081990, 2019.

Hoyle, C. R., Fuchs, C., Järvinen, E., Saathoff, H., Dias, A., El Haddad, I., Gysel, M., Coburn, S. C., Tröstl, J., Bernhammer, A.-K., Bianchi, F., Breitenlechner, M., Corbin, J. C., Craven, J., Donahue, N. M., Duplissy, J., Ehrhart, S., Frege, C., Gordon, H., Höppel, N., Heinritzi, M., Kristensen, T. B., Molteni, U., Nichman, L., Pinterich, T., Prévôt, A. S. H., Simon, M., Slowik, J. G., Steiner, G., Tomé, A., Vogel, A. L., Volkamer, R., Wagner, A. C., Wagner, R., Wexler, A. S., Williamson, C., Winkler, P. M., Yan, C., Amorim, A., Dommen, J., Curtius, J., Gallagher, M. W., Flagan, R. C., Hansel, A., Kirkby, J., Kulmala, M., Möhler, O., Stratmann, F., Worsnop, D. R., and Baltensperger, U.: Aqueous phase oxidation of sulphur dioxide by ozone in cloud droplets, Atmospheric Chem. Phys., 16, 1693–1712, https://doi.org/10.5194/acp-16-1693-2016, 2016.

Ishino, S., Hattori, S., Legrand, M., Chen, Q., Alexander, B., Shao, J., Huang, J., Jaeglé, L., Jourdain, B., Preunkert, S., Yamada, A., Yoshida, N., and Savarino, J.: Regional Characteristics of Atmospheric Sulfate Formation in East Antarctica Imprinted on 17O-Excess Signature, J. Geophys. Res. Atmospheres, 126, e2020JD033583, https://doi.org/10.1029/2020JD033583, 2021.

Jacob, D. J., Field, B. D., Li, Q., Blake, D. R., de Gouw, J., Warneke, C., Hansel, A., Wisthaler, A., Singh, H. B., and Guenther, A.: Global budget of methanol: Constraints from atmospheric observations, J. Geophys. Res. Atmospheres, 110, https://doi.org/10.1029/2004JD005172, 2005.

Jernigan, C. M., Fite, C. H., Vereecken, L., Berkelhammer, M. B., Rollins, A. W., Rickly, P. S., Novelli, A., Taraborrelli, D., Holmes, C. D., and Bertram, T. H.: Efficient Production of Carbonyl Sulfide in the Low-NOx Oxidation of Dimethyl Sulfide, Geophys. Res. Lett., 49, e2021GL096838, https://doi.org/10.1029/2021GL096838, 2022a.

Jernigan, C. M., Cappa, C. D., and Bertram, T. H.: Reactive Uptake of Hydroperoxymethyl Thioformate to Sodium Chloride and Sodium Iodide Aerosol Particles, J. Phys. Chem. A, 126, 4476–4481, https://doi.org/10.1021/acs.jpca.2c03222, 2022b.

Johnson, J. S. and Jen, C. N.: Role of Methanesulfonic Acid in Sulfuric Acid–Amine and Ammonia New Particle Formation, ACS Earth Space Chem., 7, 653–660, https://doi.org/10.1021/acsearthspacechem.3c00017, 2023.

Johnson, M. T.: A numerical scheme to calculate temperature and salinity dependent air-water transfer velocities for any gas, Ocean Sci., 6, 913–932, https://doi.org/10.5194/os-6-913-2010, 2010.

Kaufman, Y. J. and Tanré, D.: Effect of variations in super-saturation on the formation of cloud condensation nuclei, Nature, 369, 45–48, https://doi.org/10.1038/369045a0, 1994.

Khan, M. A. H., Gillespie, S. M. P., Razis, B., Xiao, P., Davies-Coleman, M. T., Percival, C. J., Derwent, R. G., Dyke, J. M., Ghosh, M. V., Lee, E. P. F., and Shallcross, D. E.: A modelling study of the atmospheric chemistry of DMS using the global model, STOCHEM-CRI, Atmos. Environ., 127, 69–79, https://doi.org/10.1016/j.atmosenv.2015.12.028, 2016.

Khan, M. A. H., Bannan, T. J., Holland, R., Shallcross, D. E., Archibald, A. T., Matthews, E., Back, A., Allan, J., Coe, H., Artaxo, P., and Percival, C. J.: Impacts of Hydroperoxymethyl Thioformate on the Global Marine Sulfur Budget, ACS Earth Space Chem., 5, 2577–2586, https://doi.org/10.1021/acsearthspacechem.1c00218, 2021.

Kloster, S., Feichter, J., Maier-Reimer, E., Six, K. D., Stier, P., and Wetzel, P.: DMS cycle in the marine ocean-atmosphere system – a global model study, Biogeosciences, 3, 29–51, https://doi.org/10.5194/bg-3-29-2006, 2006.

Kodros, J. K. and Pierce, J. R.: Important global and regional differences in aerosol cloud-albedo effect estimates between simulations with and without prognostic aerosol microphysics, J. Geophys. Res. Atmospheres, 122, 4003–4018, https://doi.org/10.1002/2016JD025886, 2017.

Kodros, J. K., Cucinotta, R., Ridley, D. A., Wiedinmyer, C., and Pierce, J. R.: The aerosol radiative effects of uncontrolled combustion of domestic waste, Atmospheric Chem. Phys., 16, 6771–6784, https://doi.org/10.5194/acp-16-6771-2016, 2016.

Kouvarakis, G. and Mihalopoulos, N.: Seasonal variation of dimethylsulfide in the gas phase and of methanesulfonate and non-sea-salt sulfate in the aerosols phase in the Eastern Mediterranean atmosphere, Atmos. Environ., 36, 929–938, https://doi.org/10.1016/S1352-2310(01)00511-8, 2002.

Kowalczuk, P., Cooper, W. J., Whitehead, R. F., Durako, M. J., and Sheldon, W.: Characterization of CDOM in an organic-rich river and surrounding coastal ocean in the South Atlantic Bight, Aquat. Sci., 65, 384–401, https://doi.org/10.1007/s00027-003-0678-1, 2003.

Kulmala, M.: How Particles Nucleate and Grow, Science, 302, 1000–1001, https://doi.org/10.1126/science.1090848, 2003.

Kulmala, M., Pirjola, L., and Mäkelä, J. M.: Stable sulphate clusters as a source of new atmospheric particles, Nature, 404, 66–69, https://doi.org/10.1038/35003550, 2000.

Lana, A., Bell, T. G., Simó, R., Vallina, S. M., Ballabrera-Poy, J., Kettle, A. J., Dachs, J., Bopp, L., Saltzman, E. S., Stefels, J., Johnson, J. E., and Liss, P. S.: An updated climatology of surface dimethlysulfide concentrations and emission fluxes in the global ocean, Glob. Biogeochem. Cycles, 25, https://doi.org/10.1029/2010GB003850, 2011.

Leaitch, W. R., Sharma, S., Huang, L., Toom-Sauntry, D., Chivulescu, A., Macdonald, A. M., von Salzen, K., Pierce, J. R., Bertram, A. K., Schroder, J. C., Shantz, N. C., Chang, R. Y.-W., and Norman, A.-L.: Dimethyl sulfide control of the clean summertime Arctic aerosol and cloud, Elem. Sci. Anthr., 1, 000017, https://doi.org/10.12952/journal.elementa.000017, 2013.

Lee, Y. H. and Adams, P. J.: A Fast and Efficient Version of the TwO-Moment Aerosol Sectional (TOMAS) Global Aerosol Microphysics Model, Aerosol Sci. Technol., 46, 678–689, https://doi.org/10.1080/02786826.2011.643259, 2012.

Lee, Y. H., Pierce, J. R., and Adams, P. J.: Representation of nucleation mode microphysics in a global aerosol model with sectional microphysics, Geosci. Model Dev., 6, 1221–1232, https://doi.org/10.5194/gmd-6-1221-2013, 2013.

Lennartz, S. T., Krysztofiak, G., Marandino, C. A., Sinnhuber, B.-M., Tegtmeier, S., Ziska, F., Hossaini, R., Krüger, K., Montzka, S. A., Atlas, E., Oram, D. E., Keber, T., Bönisch, H., and Quack, B.: Modelling marine emissions and atmospheric distributions of halocarbons and dimethyl sulfide: the influence of prescribed water concentration vs. prescribed emissions, Atmospheric Chem. Phys., 15, 11753–11772, https://doi.org/10.5194/acp-15-11753-2015, 2015.

Liu, H., Jacob, D. J., Bey, I., and Yantosca, R. M.: Constraints from 210Pb and 7Be on wet deposition and transport in a global three-dimensional chemical tracer model driven by assimilated meteorological fields, J. Geophys. Res. Atmospheres, 106, 12109–12128, https://doi.org/10.1029/2000JD900839, 2001.

Lucas, D. D. and Prinn, R. G.: Mechanistic studies of dimethylsulfide oxidation products using an observationally constrained model, J. Geophys. Res. Atmospheres, 107, ACH 12-1-ACH 12-26, https://doi.org/10.1029/2001JD000843, 2002.

Napari, I., Noppel, M., Vehkamäki, H., and Kulmala, M.: Parametrization of ternary nucleation rates for H2SO4-NH3-H2O vapors, J. Geophys. Res. Atmospheres, 107, AAC 6-1-AAC 6-6, https://doi.org/10.1029/2002JD002132, 2002.

Nightingale, P. D., Malin, G., Law, C. S., Watson, A. J., Liss, P. S., Liddicoat, M. I., Boutin, J., and Upstill-Goddard, R. C.: In situ evaluation of air-sea gas exchange parameterizations using novel conservative and volatile tracers, Glob. Biogeochem. Cycles, 14, 373–387, https://doi.org/10.1029/1999GB900091, 2000.

Novak, G. A., Fite, C. H., Holmes, C. D., Veres, P. R., Neuman, J. A., Faloona, I., Thornton, J. A., Wolfe, G. M., Vermeuel, M. P., Jernigan, C. M., Peischl, J., Ryerson, T. B., Thompson, C. R., Bourgeois, I., Warneke, C., Gkatzelis, G. I., Coggon, M. M., Sekimoto, K., Bui, T. P., Dean-Day, J., Diskin, G. S., DiGangi, J. P., Nowak, J. B., Moore, R. H., Wiggins, E. B., Winstead, E. L., Robinson, C., Thornhill, K. L., Sanchez, K. J., Hall, S. R., Ullmann, K., Dollner, M., Weinzierl, B., Blake, D. R., and Bertram, T. H.: Rapid cloud removal of dimethyl sulfide oxidation products limits SO2 and cloud condensation nuclei production in the marine atmosphere, Proc. Natl. Acad. Sci., 118, e2110472118, https://doi.org/10.1073/pnas.2110472118, 2021.

Novak, G. A., Kilgour, D. B., Jernigan, C. M., Vermeuel, M. P., and Bertram, T. H.: Oceanic emissions of dimethyl sulfide and methanethiol and their contribution to sulfur dioxide production in the marine atmosphere, Atmospheric Chem. Phys., 22, 6309–6325, https://doi.org/10.5194/acp-22-6309-2022, 2022.

Park, R. J., Jacob, D. J., Field, B. D., Yantosca, R. M., and Chin, M.: Natural and transboundary pollution influences on sulfate-nitrate-ammonium aerosols in the United States: Implications for policy, J. Geophys. Res. Atmospheres, 109, https://doi.org/10.1029/2003JD004473, 2004.

Parrella, J. P., Jacob, D. J., Liang, Q., Zhang, Y., Mickley, L. J., Miller, B., Evans, M. J., Yang, X., Pyle, J. A., Theys, N., and Van Roozendael, M.: Tropospheric bromine chemistry: implications for present and pre-industrial ozone and mercury, Atmospheric Chem. Phys., 12, 6723–6740, https://doi.org/10.5194/acp-12-6723-2012, 2012.

Pham, M., Müller, J.-F., Brasseur, G. P., Granier, C., and Mégie, G.: A three-dimensional study of the tropospheric sulfur cycle, J. Geophys. Res. Atmospheres, 100, 26061–26092, https://doi.org/10.1029/95JD02095, 1995.

Pierce, J. R. and Adams, P. J.: Global evaluation of CCN formation by direct emission of sea salt and growth of ultrafine sea salt, J. Geophys. Res. Atmospheres, 111, https://doi.org/10.1029/2005JD006186, 2006.

Pound, R. J., Sherwen, T., Helmig, D., Carpenter, L. J., and Evans, M. J.: Influences of oceanic ozone deposition on tropospheric photochemistry, Atmospheric Chem. Phys., 20, 4227–4239, https://doi.org/10.5194/acp-20-4227-2020, 2020.

Pye, H. O. T., Liao, H., Wu, S., Mickley, L. J., Jacob, D. J., Henze, D. K., and Seinfeld, J. H.: Effect of changes in climate and emissions on future sulfate-nitrate-ammonium aerosol levels in the United States, J. Geophys. Res. Atmospheres, 114, https://doi.org/10.1029/2008JD010701, 2009.

Rosati, B., Isokääntä, S., Christiansen, S., Jensen, M. M., Moosakutty, S. P., Wollesen de Jonge, R., Massling, A., Glasius, M., Elm, J., Virtanen, A., and Bilde, M.: Hygroscopicity and CCN potential of DMS-derived aerosol particles, Atmospheric Chem. Phys., 22, 13449–13466, https://doi.org/10.5194/acp-22-13449-2022, 2022.

Saunders, S. M., Jenkin, M. E., Derwent, R. G., and Pilling, M. J.: Protocol for the development of the Master Chemical Mechanism, MCM v3 (Part A): tropospheric degradation of non-aromatic volatile organic compounds, Atmospheric Chem. Phys., 3, 161–180, https://doi.org/10.5194/acp-3-161-2003, 2003.

Schmidt, J. A., Jacob, D. J., Horowitz, H. M., Hu, L., Sherwen, T., Evans, M. J., Liang, Q., Suleiman, R. M., Oram, D. E., Le Breton, M., Percival, C. J., Wang, S., Dix, B., and Volkamer, R.: Modeling the observed tropospheric BrO background: Importance of multiphase chemistry and implications for ozone, OH, and mercury, J. Geophys. Res. Atmospheres, 121, 11,819-11,835, https://doi.org/10.1002/2015JD024229, 2016.

Schobesberger, S., Junninen, H., Bianchi, F., Lönn, G., Ehn, M., Lehtipalo, K., Dommen, J., Ehrhart, S., Ortega, I. K., Franchin, A., Nieminen, T., Riccobono, F., Hutterli, M., Duplissy, J., Almeida, J., Amorim, A., Breitenlechner, M., Downard, A. J., Dunne, E. M., Flagan, R. C., Kajos, M., Keskinen, H., Kirkby, J., Kupc, A., Kürten, A., Kurtén, T., Laaksonen, A., Mathot, S., Onnela, A., Praplan, A. P., Rondo, L., Santos, F. D., Schallhart, S., Schnitzhofer, R., Sipilä, M., Tomé, A., Tsagkogeorgas, G., Vehkamäki, H., Wimmer, D., Baltensperger, U., Carslaw, K. S., Curtius, J., Hansel, A., Petäjä, T., Kulmala, M., Donahue, N. M., and Worsnop, D. R.: Molecular understanding of atmospheric particle formation from sulfuric acid and large oxidized organic molecules, Proc. Natl. Acad. Sci., 110, 17223–17228, https://doi.org/10.1073/pnas.1306973110, 2013.

Sehested, K. and Holcman, J.: A pulse radiolysis study of the OH radical induced autoxidation of methanesulfinic acid, Radiat. Phys. Chem., 47, 357–360, https://doi.org/10.1016/0969-806X(95)00115-E, 1996.

Sherwen, T., Schmidt, J. A., Evans, M. J., Carpenter, L. J., Großmann, K., Eastham, S. D., Jacob, D. J., Dix, B., Koenig, T. K., Sinreich, R., Ortega, I., Volkamer, R., Saiz-Lopez, A., Prados-Roman, C., Mahajan, A. S., and Ordóñez, C.: Global impacts of tropospheric halogens (Cl, Br, I) on oxidants and composition in GEOS-Chem, Atmospheric Chem. Phys., 16, 12239–12271, https://doi.org/10.5194/acp-16-12239-2016, 2016a.

Sherwen, T. M., Evans, M. J., Spracklen, D. V., Carpenter, L. J., Chance, R., Baker, A. R., Schmidt, J. A., and Breider, T. J.: Global modeling of tropospheric iodine aerosol, Geophys. Res. Lett., 43, 10012–10019, https://doi.org/10.1002/2016GL070062, 2016b.

Sipilä, M., Berndt, T., Petäjä, T., Brus, D., Vanhanen, J., Stratmann, F., Patokoski, J., Mauldin, R. L., Hyvärinen, A.-P., Lihavainen, H., and Kulmala, M.: The Role of Sulfuric Acid in Atmospheric Nucleation, Science, 327, 1243–1246, https://doi.org/10.1126/science.1180315, 2010.

Spracklen, D. V., Pringle, K. J., Carslaw, K. S., Chipperfield, M. P., and Mann, G. W.: A global off-line model of size-resolved aerosol microphysics: I. Model development and prediction of aerosol properties, Atmospheric Chem. Phys., 5, 2227–2252, https://doi.org/10.5194/acp-5-2227-2005, 2005.

Thomas, M. A., Suntharalingam, P., Pozzoli, L., Rast, S., Devasthale, A., Kloster, S., Feichter, J., and Lenton, T. M.: Quantification of DMS aerosol-cloud-climate interactions using the ECHAM5-HAMMOZ model in a current climate scenario, Atmospheric Chem. Phys., 10, 7425–7438, https://doi.org/10.5194/acp-10-7425-2010, 2010.

Trivitayanurak, W., Adams, P. J., Spracklen, D. V., and Carslaw, K. S.: Tropospheric aerosol microphysics simulation with assimilated meteorology: model description and intermodel comparison, Atmospheric Chem. Phys., 8, 3149–3168, https://doi.org/10.5194/acp-8-3149-2008, 2008.

Vehkamäki, H., Kulmala, M., Napari, I., Lehtinen, K. E. J., Timmreck, C., Noppel, M., and Laaksonen, A.: An improved parameterization for sulfuric acid–water nucleation rates for tropospheric and stratospheric conditions, J. Geophys. Res. Atmospheres, 107, AAC 3-1-AAC 3-10, https://doi.org/10.1029/2002JD002184, 2002.

Veres, P. R., Neuman, J. A., Bertram, T. H., Assaf, E., Wolfe, G. M., Williamson, C. J., Weinzierl, B., Tilmes, S., Thompson, C. R., Thames, A. B., Schroder, J. C., Saiz-Lopez, A., Rollins, A. W., Roberts, J. M., Price, D., Peischl, J., Nault, B. A., Møller, K. H., Miller, D. O., Meinardi, S., Li, Q., Lamarque, J.-F., Kupc, A., Kjaergaard, H. G., Kinnison, D., Jimenez, J. L., Jernigan, C. M., Hornbrook, R. S., Hills, A., Dollner, M., Day, D. A., Cuevas, C. A., Campuzano-Jost, P., Burkholder, J., Bui, T. P., Brune, W. H., Brown, S. S., Brock, C. A., Bourgeois, I., Blake, D. R., Apel, E. C., and Ryerson, T. B.: Global airborne sampling reveals a previously unobserved dimethyl sulfide oxidation mechanism in the marine atmosphere, Proc. Natl. Acad. Sci., 117, 4505–4510, https://doi.org/10.1073/pnas.1919344117, 2020.

Vermeuel, M. P., Novak, G. A., Jernigan, C. M., and Bertram, T. H.: Diel Profile of Hydroperoxymethyl Thioformate: Evidence for Surface Deposition and Multiphase Chemistry, Environ. Sci. Technol., 54, 12521–12529, https://doi.org/10.1021/acs.est.0c04323, 2020.

Wang, W.-L., Song, G., Primeau, F., Saltzman, E. S., Bell, T. G., and Moore, J. K.: Global ocean dimethyl sulfide climatology estimated from observations and an artificial neural network, Biogeosciences, 17, 5335–5354, https://doi.org/10.5194/bg-17-5335-2020, 2020.

Wang, X., Jacob, D. J., Eastham, S. D., Sulprizio, M. P., Zhu, L., Chen, Q., Alexander, B., Sherwen, T., Evans, M. J., Lee, B. H., Haskins, J. D., Lopez-Hilfiker, F. D., Thornton, J. A., Huey, G. L., and Liao, H.: The role of chlorine in global tropospheric chemistry, Atmospheric Chem. Phys., 19, 3981–4003, https://doi.org/10.5194/acp-19-3981-2019, 2019.

Wang, X., Jacob, D. J., Downs, W., Zhai, S., Zhu, L., Shah, V., Holmes, C. D., Sherwen, T., Alexander, B., Evans, M. J., Eastham, S. D., Neuman, J. A., Veres, P. R., Koenig, T. K., Volkamer, R., Huey, L. G., Bannan, T. J., Percival, C. J., Lee, B. H., and Thornton, J. A.: Global tropospheric halogen (Cl, Br, I) chemistry and its impact on oxidants, Atmospheric Chem. Phys., 21, 13973–13996, https://doi.org/10.5194/acp-21-13973-2021, 2021.

Wang, Y., Jacob, D. J., and Logan, J. A.: Global simulation of tropospheric O3-NO x - hydrocarbon chemistry: 1. Model formulation, J. Geophys. Res. Atmospheres, 103, 10713–10725, https://doi.org/10.1029/98JD00158, 1998.

Wesely, M. L.: Parameterization of surface resistances to gaseous dry deposition in regional-scale numerical models, Atmospheric Environ. 1967, 23, 1293–1304, https://doi.org/10.1016/0004-6981(89)90153-4, 1989.

Westervelt, D. M., Pierce, J. R., Riipinen, I., Trivitayanurak, W., Hamed, A., Kulmala, M., Laaksonen, A., Decesari, S., and Adams, P. J.: Formation and growth of nucleated particles into cloud condensation nuclei: model–measurement comparison, Atmospheric Chem. Phys., 13, 7645–7663, https://doi.org/10.5194/acp-13-7645-2013, 2013.

Williamson, C. J., Kupc, A., Axisa, D., Bilsback, K. R., Bui, T., Campuzano-Jost, P., Dollner, M., Froyd, K. D., Hodshire, A. L., Jimenez, J. L., Kodros, J. K., Luo, G., Murphy, D. M., Nault, B. A., Ray, E. A., Weinzierl, B., Wilson, J. C., Yu, F., Yu, P., Pierce, J. R., and Brock, C. A.: A large source of cloud condensation nuclei from new particle formation in the tropics, Nature, 574, 399–403, https://doi.org/10.1038/s41586-019-1638-9, 2019.

Wollesen de Jonge, R., Elm, J., Rosati, B., Christiansen, S., Hyttinen, N., Lüdemann, D., Bilde, M., and Roldin, P.: Secondary aerosol formation from dimethyl sulfide – improved mechanistic understanding based on smog chamber experiments and modelling, Atmospheric Chem. Phys., 21, 9955–9976, https://doi.org/10.5194/acp-21-9955-2021, 2021.

Wu, R., Wang, S., and Wang, L.: New Mechanism for the Atmospheric Oxidation of Dimethyl Sulfide. The Importance of Intramolecular Hydrogen Shift in a CH3SCH2OO Radical, J. Phys. Chem. A, 119, 112–117, https://doi.org/10.1021/jp511616j, 2015.

Zhang, J.-Z. and Millero, F. J.: The products from the oxidation of H2S in seawater, Geochim. Cosmochim. Acta, 57, 1705–1718, https://doi.org/10.1016/0016-7037(93)90108-9, 1993.

Zhang, Y., Jacob, D. J., Maasakkers, J. D., Sulprizio, M. P., Sheng, J.-X., Gautam, R., and Worden, J.: Monitoring global tropospheric OH concentrations using satellite observations of atmospheric methane, Atmospheric Chem. Phys., 18, 15959–15973, https://doi.org/10.5194/acp-18-15959-2018, 2018.

Zhou, Z.-X., Lujan, S. A., Burkholder, A. B., Garbacz, M. A., and Kunkel, T. A.: Roles for DNA polymerase δ in initiating and terminating leading strand DNA replication, Nat. Commun., 10, 3992, https://doi.org/10.1038/s41467-019-11995-z, 2019.

Zhu, L., Nicovich, J. M., and Wine, P. H.: Temperature-dependent kinetics studies of aqueous phase reactions of hydroxyl radicals with dimethylsulfoxide, dimethylsulfone, and methanesulfonate, Aquat. Sci., 65, 425–435, https://doi.org/10.1007/s00027-003-0673-6, 2003.

Zhu, L., Nenes, A., Wine, P. H., and Nicovich, J. M.: Effects of aqueous organosulfur chemistry on particulate methanesulfonate to non–sea salt sulfate ratios in the marine atmosphere, J. Geophys. Res. Atmospheres, 111, https://doi.org/10.1029/2005JD006326, 2006.

Zhu, L., Jacob, D. J., Eastham, S. D., Sulprizio, M. P., Wang, X., Sherwen, T., Evans, M. J., Chen, Q., Alexander, B., Koenig, T. K., Volkamer, R., Huey, L. G., Le Breton, M., Bannan, T. J., and Percival, C. J.: Effect of sea salt aerosol on tropospheric bromine chemistry, Atmospheric Chem. Phys., 19, 6497–6507, https://doi.org/10.5194/acp-19-6497-2019, 2019.